J. Fluid Mech. (1992), *vol.* 240, *pp.* 197–228
Printed in Great Britain

Transonic flows of Bethe–Zel'dovich–Thompson fluids

By M. S. CRAMER[1] AND G. M. TARKENTON[2]

[1] Department of Engineering Science and Mechanics, Virginia Polytechnic Institute and State University, Blacksburg, VA 24061–0219, USA

[2] Department of Physics, University of Texas at Austin, Austin, TX 78741, USA

(Received 26 July 1991)

Bethe–Zel'dovich–Thompson fluids are ordinary, single-phase fluids in which the fundamental derivative of gasdynamics is negative over a finite range of temperatures and pressures. We examine the steady transonic flow of these fluids over two-dimensional thin wings and turbine blades. The free-stream state is taken to be in the neighbourhood of one of the zeros of the fundamental derivative. It is shown that a modified form of the classical transonic small-disturbance equation governs such flows. Critical Mach number estimates are provided which take into account the non-monotone variation of the Mach number with pressure predicted in previous investigations. Critical Mach numbers well over 0.95 are predicted for conventional airfoil sections. Numerical solutions reveal substantial reductions in the strength of the compression shocks occurring in supercritical flows. Further new results include the prediction of expansion and compression shocks in the same flow and compression bow shocks in flows with subsonic free streams.

1. Introduction

Transonic flows are characterized by significantly larger losses than those corresponding to the subsonic and low supersonic regime. An important component of these losses is that due to the formation of shock waves on the wing or turbine blade. In addition to the irreversibility of the shocks themselves, the strong adverse pressure gradients can lead to boundary-layer separation. The resultant vibration and noise can also have serious consequences in the operation of modern turbomachinery.

Efforts to reduce these losses or to narrow the range of transonic Mach numbers are hindered by the fact that shock formation is due to the intrinsic nonlinearity of the fluid. A convenient measure of this nonlinearity is the thermodynamic parameter

$$\Gamma \equiv \frac{1}{\rho}\frac{\partial(\rho a)}{\partial \rho}\bigg|_s = \frac{a}{\rho} + \frac{\partial a}{\partial \rho}\bigg|_s, \tag{1.1}$$

where ρ and s are the fluid density and entropy and

$$a \equiv \left[\frac{\partial p}{\partial \rho}\bigg|_s\right]^{\frac{1}{2}} \tag{1.2}$$

is the thermodynamic sound speed. Here $p = p(\rho, s)$ is the fluid pressure. This parameter was first introduced by Duhem (1909) in his analysis of the shock admissibility conditions for general fluids. Thompson (1971) has demonstrated the

significance of Γ to a wide range of compressible flows. For this reason, Thompson has referred to (1.1) as the fundamental derivative of gasdynamics. Perhaps the earliest discussion of the fundamental derivative in the context of transonic flows is due to Hayes (1966) who demonstrated that the classical transonic similarity parameter may be written

$$K_1 = \frac{1-M_\infty^2}{(\bar{\Gamma}\epsilon)^{\frac{2}{3}}}, \tag{1.3}$$

where M_∞ is the free-stream Mach number, ϵ is a small parameter measuring the thickness or angle of attack of the wing or blade and

$$\bar{\Gamma} \equiv \frac{\Gamma_\infty \rho_\infty}{a_\infty} \tag{1.4}$$

is a non-dimensional version of Γ, evaluated at the thermodynamic state of the free stream. If we consider perfect gases, i.e. those satisfying

$$p = \rho R T \tag{1.5}$$

with

$$c_v = \text{constant}, \tag{1.6}$$

where R is the gas constant, T is the absolute temperature and c_v is the specific heat at constant volume, we find that

$$\Gamma = \frac{a}{\rho}\frac{\gamma+1}{2} \quad \text{and therefore} \quad \bar{\Gamma} = \frac{\gamma_\infty+1}{2}, \tag{1.7}$$

where γ is the usual ratio of specific heats. The well-known conditions for the thermodynamic stability of any fluid require

$$c_v(\rho, T) > 0 \quad \text{and} \quad \frac{\partial p}{\partial \rho}(\rho, T) > 0 \tag{1.8}$$

which, in turn, require that $\gamma > 1$. As a result, $\bar{\Gamma} > 1$ if the gas is perfect. Owing to this lower bound on $\bar{\Gamma}$, the critical Mach number of perfect gases tends to be in the general range 0.6–0.8 for typical two-dimensional airfoil profiles at small angles of attack. By critical Mach number we mean the free-stream Mach number at which regions of supersonic flow, and therefore shock waves, first appear. Although shock-free configurations have been developed such solutions tend to be isolated and give rise to strong shocks in the neighbourhood of the design point. Summaries of the relevant design strategies have been reviewed by Nieuwland & Spee (1971) and Sobieczky & Seebass (1984).

When the densities and temperatures are in the general neighbourhood of those corresponding to the thermodynamic critical point, it is well-known that the ideal gas model (1.5) no longer gives an accurate quantitative or even qualitative approximation to the actual fluid response. A more complex equation of state, such as that due to van der Waals, is required to model even the qualitative behaviour. In this dense gas regime it is found that the sound speed of most fluids decreases with isentropic increases of the density. From (1.1) it is clear that $\rho\Gamma/a < 1$ in this region, thus resulting in a significant reduction in the intrinsic nonlinearity of the fluid. As an example of this reduction, we compare the values of $\rho\Gamma/a$ for ordinary octane (C_8H_{18}) as obtained in the low-pressure and dense gas regimes. If we employ the physical property data given by Reid, Prausnitz & Poling (1987), we find that the low-pressure, i.e. perfect gas, sound speed of octane is approximately 210 m/s at

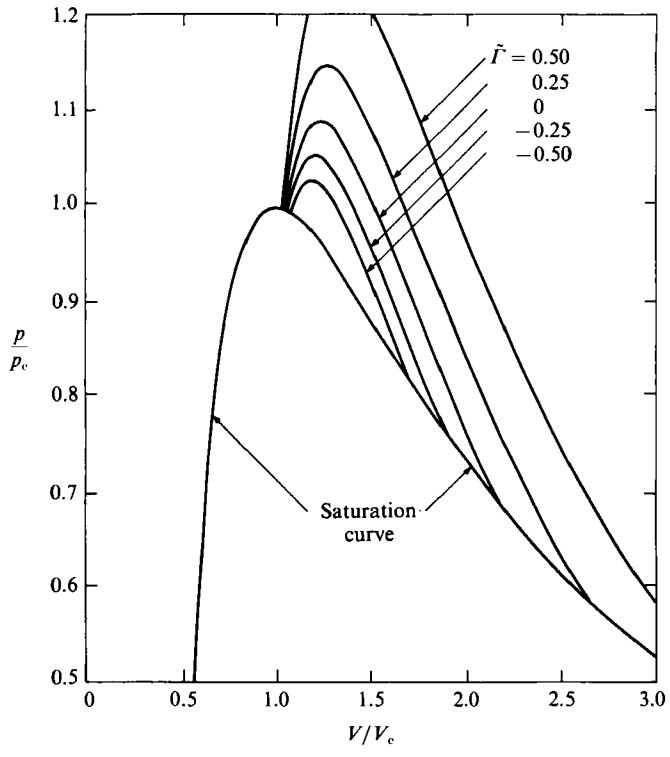

FIGURE 1. Constant $\tilde{\Gamma} \equiv \rho\Gamma/a$ contours. Fluid is a van der Waals gas with $c_v = 50R$.

octane's critical temperature of 587 K. The corresponding value of $\rho\Gamma/a$ is approximately 1.01. If we employ the well-known Martin–Hou equation of state (Martin & Hou 1955) we find that the sound speed is only about 95 m/s at the same temperature but at a density of about half the critical value, i.e. at approximately 0.115 gm/cc. The corresponding value of $\rho\Gamma/a$ is found to be 0.41 which is seen to be about 40% of the low-pressure value and about a third of the value found for a perfect diatomic ($\gamma = 1.4$) gas. If we consider a wing for which the critical value of K_1 is 3.0 and $\epsilon = 0.06$ we find that the critical Mach number in the dense gas case is approximately 18% larger than the low-pressure result for octane.

Even more dramatic differences with the perfect gas theory are seen in fluids in which the decrease in the sound speed is so large that the fundamental derivative becomes negative. This region of negative Γ is depicted in figure 1 where constant $\tilde{\Gamma} \equiv \rho\Gamma/a$ contours have been computed and plotted for the case of a van der Waals gas with constant specific heat c_v. The fact that fluids which have sufficiently large specific heats will possess a region of negative Γ was first pointed out by Bethe (1942) and Zel'dovich (1946). More detailed studies were carried out by Lambrakis & Thompson (1972), Thompson & Lambrakis (1973), and Cramer (1989*a*) who employed highly accurate equations of state to identify a wide range of negative-Γ fluids of practical interest. One such example is the common heat transfer fluid referred to as FC-70. The variation of $\rho\Gamma/a$ on isotherms has been computed and plotted for FC-70 in figure 2. Because of the significance of these early studies, we refer to fluids which have a region of negative Γ similar to that depicted in figures 1 and 2 as Bethe–Zel'dovich–Thompson (BZT) fluids.

The first to examine near-sonic flows of BZT fluids was Thompson (1971) who

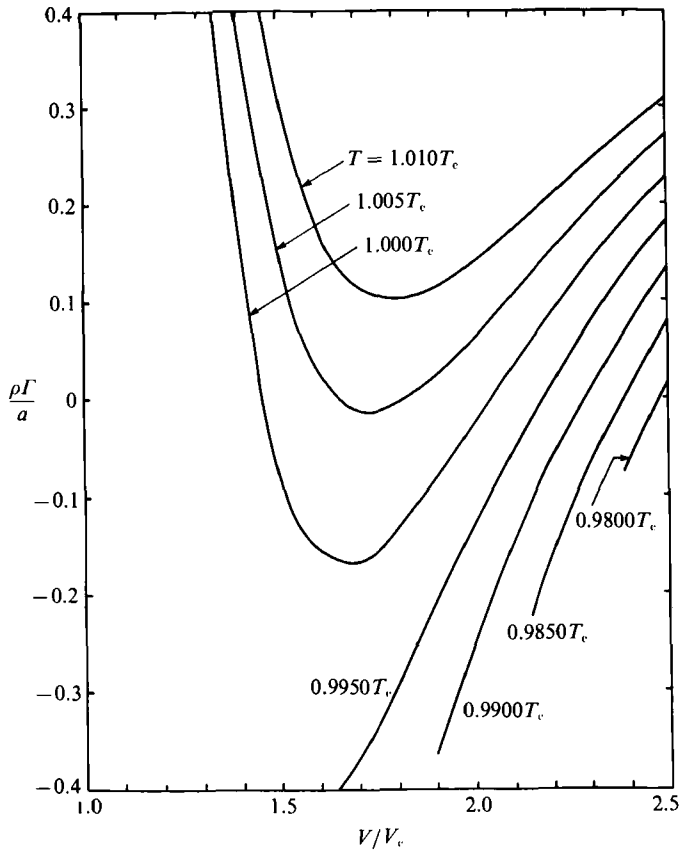

FIGURE 2. Computed values of $\rho\Gamma/a$ along isotherms for FC-70 (perfluoro-tripentylamine). Equation of state used is due to Martin & Hou (1955). Full details are found in Cramer (1989*a*).

derived the following relation between the fundamental derivative and the area variation of a duct or streamtube:

$$\left[\frac{\mathrm{d}M}{\mathrm{d}x}\right]^2_{M=1} = \frac{1}{2}\left[\frac{\rho\Gamma}{a}\frac{1}{A}\frac{\mathrm{d}^2A}{\mathrm{d}x^2}\right]_{M=1}, \tag{1.9}$$

where $A = A(x)$ is the streamtube area and M is the Mach number. From (1.9) and the well-known fact that the streamtube area has an extremum at the sonic condition it may be shown that supersonic flow may be attained only by way of a throat, i.e., $\mathrm{d}^2A/\mathrm{d}x^2 > 0$, if $\Gamma > 0$ and by way of an anti-throat, i.e., a local maximum in the streamtube area, if $\Gamma < 0$. Thompson (1971), Cramer (1991), and Cramer & Best (1991) also demonstrated that the flow cannot be accelerated isentropically from stagnation conditions, i.e. those having $M = 0$, if $\Gamma < 0$ at every point in the flow. These results clearly suggest that the onset of supersonic flow will be delayed in the negative-Γ region. One of the main objectives of the present investigation is to verify and quantify this assertion.

The work of Duhem (1909), Bethe (1942), Zel'dovich (1946), Thompson (1971), Thompson & Lambrakis (1973), Pego (1986), Menikoff & Plohr (1989), and Cramer (1991) demonstrates that the fundamental existence issues for shock waves are significantly more complicated when BZT fluids are considered. When $\Gamma < 0$ at every point in the flow, the well-known compression shocks of the perfect gas theory violate

the entropy inequality and will disintegrate if inserted in the flow. The disintegration into a centred compression fan in the context of steady supersonic flows was first described by Thompson (1971). Elementary shock formation studies, examples of which are found in Landau & Lifschitz (1959), demonstrate that such shocks will not form from smooth initial conditions. Thus, even when the critical Mach number is exceeded, the strong adverse pressure gradients associated with compression shocks will not occur and it appears that shock-induced separation may be eliminated completely in flows having $\Gamma < 0$ at every point.

Although compression shocks disintegrate in $\Gamma < 0$ regions, expansion shocks, forbidden in the perfect gas theory, satisfy all the relevant admissibility conditions and are expected to occur in supercritical flows in which $\Gamma < 0$ at every point.

If the fundamental derivative changes sign in the flow, both expansion and compression shocks may exist in the same flow. On the other hand, both compression and expansion shocks not satisfying the basic existence criteria may disintegrate either completely or in part. Examples of the partial disintegration processes are found in the work of Wendroff (1972), Cramer & Kluwick (1984), Cramer *et al.* (1986), Cramer & Sen (1987), Kluwick & Koller (1988), Cramer (1989*b*), Menikoff & Plohr (1989), and Cramer (1991). Thus, the adverse pressure gradients may be reduced even under the relatively weak condition that $\Gamma < 0$ only in part of the flow.

Further evidence of the complex nature of transonic flows of BZT fluids is found in the nozzle flow studies of Leidner (1990), Chandrasekar & Prasad (1991), Cramer & Best (1991), and Warner (1990). The first and third studies were restricted to isentropic flows. The remaining articles included the effects of normal shock waves in quasi-one-dimensional flows. In particular, Chandrasekar & Prasad developed an extension of the weak shock theory of Cramer & Kluwick (1984) to study the flow in the neighbourhood of both throats and anti-throats with $M \approx 1$ and $\Gamma \approx 0$. The various flow patterns were delineated, the most complex of which included both compression and expansion shocks in the same flow. The critical role of sonic shocks, i.e. shocks having a Mach number identically equal to one either upstream or downstream of the shock, was also revealed. The report by Warner extends the analysis of Cramer & Best (1991) to include finite-amplitude normal shocks. It was found that a total of three shocks – two compression and one expansion – could occur in conventional converging–diverging nozzles. This contrasts with the perfect gas theory where only one shock may appear and the small-disturbance theory of Chandrasekar & Prasad (1991) which can have a maximum of two shocks.

Results of direct interest in the present study are described by Leidner (1990), Cramer (1991), and Cramer & Best (1991). In these studies, it was shown that the Mach number may increase with density if $\bar{\Gamma} < 1$. This contrasts with the perfect gas theory where the Mach number always increases during isentropic expansions. A sketch of the Mach number variation of BZT fluids is provided in figure 3. Each curve may be considered as originating at the same thermodynamic state but with different values of the Mach number. Thus, the entropy is not only constant along each curve but from curve to curve. The work of Leidner (1990) and Cramer & Best (1991) reveals that the same general behaviour can also be observed even if each curve is a different isentrope. At pressures and temperatures such that the corresponding value of Γ is negative, the non-classical variation of the Mach number may also be observed at subsonic speeds. It would therefore appear possible to find flow conditions under which the expansion over a wing or turbine blade may actually lead to a decrease in the local Mach number which, in turn, would be expected to delay the onset of supersonic flow.

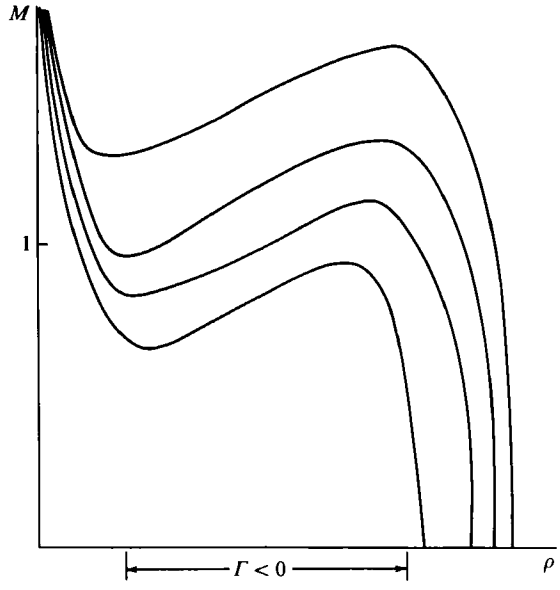

FIGURE 3. Sketch of Mach number variation in BZT fluids.

A second effect of the non-classical variation of the Mach number is related to the fact that the classical approach for the prediction of the critical Mach number depends on the assumption that the Mach number decreases monotonically with increasing density or pressure. This assumption is no longer valid when BZT fluids are considered and a fundamentally different estimation scheme is clearly required. In fact, inspection of figure 3 clearly reveals that the flow may become supersonic even in regions of compression. Cramer & Best (1991) have argued that the latter effect should give rise to bow shocks in flows having subsonic free streams. The present study provides detailed numerical evidence supporting their claim.

Numerical studies of external transonic flows have been carried out by Morren (1991). In this investigation, numerical solutions to the full Euler equations were obtained. The gas model was taken to be that due to van der Waals. Significant increases in the critical Mach number were reported which naturally resulted in very large increases in the lift to wave-drag ratios.

The present study examines the details of external transonic flows over thin wings and turbine blades. The usual assumption of small disturbances to a near-sonic free stream will be employed. A fundamental difference between this and the classical approaches is that we will make the additional assumption that the undisturbed state is in the vicinity of one of the zeros of Γ. In particular, we require that

$$\bar{\Gamma} = O\left[\frac{\rho - \rho_\infty}{\rho_\infty}\right] = o(1). \tag{1.10}$$

This assumption is equivalent to that employed by Cramer & Kluwick (1984), Cramer *et al.* (1986), Kluwick & Koller (1988), and Chandrasekar & Prasad (1991). When (1.10) holds, the local value of Γ can change sign even though the density perturbations are small. It will be seen that the non-monotone Mach number variation will also be contained in the present theory.

The general approach will be to derive a transonic small-disturbance equation governing the flow. As in the previous investigations of flows in which the fundamental derivative is small, terms which were correctly neglected in the

$\bar{\Gamma} = O(1)$ theory may make a non-negligible effect when $\bar{\Gamma}$ is small. The modified form of the small-disturbance equation has been given by Cramer (1991); the detailed derivation of this equation is provided in §3 of the present study. A scheme for the estimation of the critical Mach number is provided in §6. We also present numerical solutions to the modified transonic small-disturbance equation. The numerical approximation scheme is outlined in §7 and the results are presented in §8.

The principal advantage of the present approach over purely numerical studies is that the analytical structure is easily revealed. Furthermore, the non-classical effects may be delineated in a straightforward manner because these are controlled by a single thermodynamic parameter. The simplicity of the small-disturbance equation also means that numerical solutions may be obtained efficiently and cheaply even in the far field.

The results presented here will include the prediction of large increases in the critical Mach number and reductions in the strength of compression shocks occurring in supercritical flows. These results strongly suggest that there are significant gasdynamic advantages in the use of BZT fluids in turbomachinery. The most appropriate applications appear to be closed systems referred to as organic Rankine cycles. These systems routinely exploit the advantageous thermodynamic properties of heavy hydrocarbons and fluorocarbons of the same general type as the BZT fluids identified by Lambrakis & Thompson (1972), Thompson & Lambrakis (1973), and Cramer (1989*a*).

2. Formulation

We consider the steady, inviscid, two-dimensional flow over a single turbine blade or airfoil as sketched in figure 4. The flow far ahead of the blade is taken to be uniform at speed U_∞, density ρ_∞, and entropy s_∞. The coordinate system is taken so that the positive x-axis is aligned with the free-stream velocity. The chord and maximum thickness of the blade or airfoil are taken to be L and ϵL so that the blade surface can be written

$$y = \epsilon L F^{\pm}(x/L) \quad \text{for} \quad -\tfrac{1}{2} \leqslant x/L \leqslant \tfrac{1}{2}, \tag{2.1}$$

where the $\pm$ signs refer to the upper and lower surfaces and $F^{\pm}$ are taken to be sufficiently smooth functions of x/L. The thickness parameter ϵ will eventually be taken to be small.

Because the free stream is uniform and steady and viscous effects are neglected, the only source of entropy gradients are those generated by shock waves. Cramer & Kluwick (1984) have shown that the entropy rise is of fourth, rather than third, order in the shock strength whenever (1.10) holds. In the following it will be shown that this fact permits us to ignore the entropy variations, even though higher-order approximations are required. Furthermore, the relatively weak entropy jump leads us to expect that the vorticity generated at the shocks is also negligible. Thus, we will take the flow to be irrotational, at least to the approximation required here. Once the appropriate scalings are determined, Crocco's theorem may be employed to give an *a posteriori* justification of this approximation.

The boundary-value problem governing this irrotational flow may therefore be written

$$(\phi_x^2 - a^2)\,\phi_{xx} + 2\phi_x\,\phi_y\,\phi_{xy} + (\phi_y^2 - a^2)\,\phi_{yy} = 0, \tag{2.2}$$

$$\phi_y = \epsilon \phi_x F^{\pm\prime}, \quad \text{on} \quad y = \epsilon L F^{\pm} \quad \text{for} \quad -\tfrac{1}{2} \leqslant x/L \leqslant \tfrac{1}{2}, \tag{2.3}$$

$$\nabla\phi \to U_\infty \boldsymbol{i} \quad \text{as} \quad x^2 + y^2 \to \infty, \tag{2.4}$$

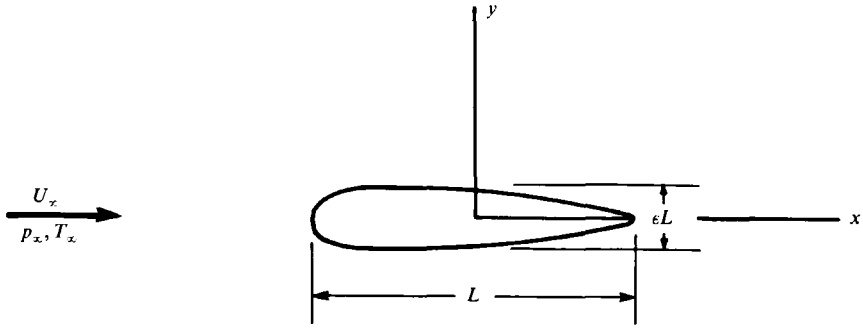

FIGURE 4. Sketch of typical wing or turbine blade and coordinate system.

where ϕ is the velocity potential defined so that $\boldsymbol{v} = \boldsymbol{\nabla}\phi$ is the fluid velocity, $F^{\pm\prime}(\zeta) \equiv \mathrm{d}F^{\pm}/\mathrm{d}\zeta$ and $a(\rho, s)$ is the thermodynamic sound speed given in (1.2). The first equation is recognized as the two-dimensional version of the exact potential equation. The second is the kinematic boundary condition at the blade and the third requires that the disturbances vanish far from the blade or wing. The disturbances in the sound speed will be related to those in ϕ by the Bernoulli equation for steady, isentropic flow, i.e.

$$h(\rho, s_\infty) = h_\infty + \tfrac{1}{2}(U_\infty^2 - |\boldsymbol{\nabla}\phi|^2), \tag{2.5}$$

where $h_\infty \equiv h(\rho_\infty, s_\infty)$ is the enthalpy. Again we note that the assumption of isentropic flow implicit in (2.5) will be valid to fourth order in the pressure or density disturbance.

In the next section it will be convenient to employ a non-dimensional form of (2.2)–(2.5). We therefore introduce the following non-dimensional variables:

$$\bar{x} \equiv \frac{x}{L}, \quad \bar{y} = \frac{y}{L}, \quad \bar{\phi} \equiv \frac{\phi - U_\infty x}{U_\infty L}, \quad \bar{a} \equiv \frac{a}{a_\infty}, \tag{2.6}$$

where $\bar{\phi} = \bar{\phi}(\bar{x}, \bar{y})$ is the non-dimensional disturbance potential and $a_\infty \equiv a(\rho_\infty, s_\infty)$. Substitution of (2.6) in (2.2)–(2.5) yields

$$(M_\infty^2 + 2M_\infty^2\bar{\phi}_{\bar{x}} + M_\infty^2\bar{\phi}_{\bar{x}}^2 - \bar{a}^2)\bar{\phi}_{\bar{x}\bar{x}} + 2M_\infty^2(1+\bar{\phi}_{\bar{x}})\bar{\phi}_{\bar{y}}\bar{\phi}_{\bar{x}\bar{y}} = (\bar{a}^2 - M_\infty^2\bar{\phi}_{\bar{y}}^2)\bar{\phi}_{\bar{y}\bar{y}}, \tag{2.7}$$

with
$$\bar{\phi}_{\bar{y}} = \epsilon(1+\bar{\phi}_{\bar{x}})F^{\pm\prime} \quad \text{on} \quad \bar{y} = \epsilon F^{\pm} \quad \text{for} \quad -\tfrac{1}{2} \leqslant \bar{x} \leqslant \tfrac{1}{2}, \tag{2.8}$$

$$\bar{\phi}_{\bar{x}}, \bar{\phi}_{\bar{y}} \to 0 \quad \text{as} \quad \bar{x}^2 + \bar{y}^2 \to \infty, \tag{2.9}$$

$$\frac{h - h_\infty}{a_\infty^2} = -M_\infty^2\{\bar{\phi}_{\bar{x}} + \tfrac{1}{2}\bar{\phi}_{\bar{x}}^2 + \tfrac{1}{2}\bar{\phi}_{\bar{y}}^2\}. \tag{2.10}$$

Equations (2.7)–(2.10) are recognized as the counterparts of (2.2)–(2.5), respectively.

3. Derivation of the transonic small-disturbance equation

In order to derive the approximate form of the exact equations presented in §2, we now formally require the wing to be thin, i.e.

$$\epsilon \ll 1, \tag{3.1}$$

the disturbances caused by it to be small, i.e.

$$\frac{\rho - \rho_\infty}{\rho_\infty}, \bar{\phi}_{\bar{x}}, \bar{\phi}_{\bar{y}} \ll 1, \tag{3.2}$$

and the flow to be nearly sonic, i.e.

$$|M_\infty^2 - 1| \ll 1. \tag{3.3}$$

Conditions (3.1)–(3.3) are just those of the classical transonic theory. As pointed out in §1, we will also employ (1.10) in order to determine the approximation in the vicinity of the $\Gamma = 0$ locus. In the following development we will derive only the lowest-order version of the $\Gamma \approx 0$ equation.

We begin by deriving the approximate relation between the non-dimensional sound speed $\bar{a}$ and the perturbations in $\bar{\phi}$. A straightforward Taylor series expansion of $h(\rho, s)$ and $a(\rho, s)$ for small $(\rho - \rho_\infty)/\rho_\infty$ and use of the assumption that $s - s_\infty = 0(\rho - \rho_\infty)^4$ yields

$$(h - h_\infty)/a_\infty^2 = \bar{\rho} - \tfrac{3}{2}\bar{\rho}^2 + O(\bar{\rho}^3), \tag{3.4}$$

$$\bar{a}^2 = a^2/a_\infty^2 = 1 - 2\bar{\rho} + 2\bar{\Gamma}\bar{\rho} + (\Lambda + 3)\bar{\rho}^2 + O(\bar{\rho}^3), \tag{3.5}$$

where

$$\Lambda \equiv \frac{\rho_\infty^2}{a_\infty}\frac{\partial \Gamma}{\partial \rho}(\rho_\infty, s_\infty) = O(1). \tag{3.6}$$

The quantity Λ is the second (cubic) nonlinearity parameter introduced by Cramer & Kluwick (1984). This parameter was also introduced by Hayes (1966) in the context of higher approximations to the classical theory. It is also useful to note that the terms involving $\bar{\Gamma}$ and $\Lambda + 3$ are both of order $\bar{\rho}^2$ due to (1.10) and (3.6). In the derivation of (3.4)–(3.5) we have also employed Gibbs' equation

$$\mathrm{d}h = T\mathrm{d}s + \frac{1}{\rho}\mathrm{d}p,$$

where T is the absolute temperature, along with (1.1)–(1.2), to show that

$$\left.\begin{aligned} \left.\frac{\partial h}{\partial \rho}\right|_s &= \frac{a^2}{\rho}, \quad \frac{\partial^2 h}{\partial \rho^2} = \frac{a^2}{\rho^2}\left[2\frac{\rho\Gamma}{a} - 3\right], \\ \frac{\partial^3 h}{\partial \rho^3} &= \frac{2a^2}{\rho^3}\left\{\frac{\rho\Gamma}{a}\left[\frac{\rho\Gamma}{a} - 5\right] + 6 + \frac{\rho^2}{a}\frac{\partial \Gamma}{\partial \rho}\right\}; \end{aligned}\right\} \tag{3.7}$$

and

$$\frac{\partial a^2}{\partial \rho} = \frac{\partial h}{\partial \rho} + \rho\frac{\partial^2 h}{\partial \rho^2}, \quad \frac{\partial^2 a^2}{\partial \rho^2} = 2\frac{\partial^2 h}{\partial \rho^2} + \rho\frac{\partial^3 h}{\partial \rho^3}. \tag{3.8}$$

We now substitute (3.4) in the exact Bernoulli equation (2.10) to yield

$$\bar{\rho} = \tfrac{3}{2}\bar{\rho}^2 - M_\infty^2(\bar{\phi}_{\bar{x}} + \tfrac{1}{2}\bar{\phi}_{\bar{x}}^2 + \tfrac{1}{2}\bar{\phi}_{\bar{y}}^2) + o(\bar{\rho}^2). \tag{3.9}$$

At this stage it is necessary to determine the relative sizes of the $\bar{x}$ and $\bar{y}$ derivatives. Here we will take

$$\bar{y} = O\left[\frac{\bar{x}}{|1 - M_\infty^2|^{\frac{1}{2}}}\right], \tag{3.10a}$$

which implies

$$\frac{\partial}{\partial \bar{y}} = O\left[|1 - M_\infty^2|^{\frac{1}{2}}\frac{\partial}{\partial \bar{x}}\right] \ll \frac{\partial}{\partial \bar{x}}. \tag{3.10b}$$

The scalings (3.10) can be motivated by requiring that our resultant transonic equation reduces to the usual wave equation

$$\left[M_\infty^2 - 1\right]\bar{\phi}_{\bar{x}\bar{x}} = \bar{\phi}_{\bar{y}\bar{y}}$$

when all nonlinear terms are neglected. Alternatively, one can examine the exact characteristic relations for supersonic flow.

When (3.10) is applied to (3.9) we find that

$$\bar{\rho} \approx -M_\infty^2 \bar{\phi}_{\bar{x}} \approx -\bar{\phi}_{\bar{x}}, \tag{3.11}$$

to lowest order, which, as one might expect, is identical to the corresponding relation of the classical theory. Thus, $\bar{\rho}$, $\bar{\Gamma}$, and $\bar{\phi}_{\bar{x}}$ are all of the same order of magnitude. We may now rewrite (3.9), and consequently (3.5), as follows:

$$\bar{\rho} = -\bar{\phi}_{\bar{x}} + \bar{\phi}_{\bar{x}}^2 + o(\bar{\phi}_{\bar{x}}^2, M_\infty^2 - 1), \tag{3.12}$$

$$\bar{a}^2 = 1 + 2\bar{\phi}_{\bar{x}} - 2\bar{\Gamma}\bar{\phi}_{\bar{x}} + (\Lambda + 1)\bar{\phi}_{\bar{x}}^2 + o(\bar{\phi}_{\bar{x}}^2, M_\infty^2 - 1). \tag{3.13}$$

In a like manner, the coefficient of the $\bar{\phi}_{\bar{x}\bar{x}}$ term in (2.7) may be approximated by

$$M_\infty^2 - 1 + 2\bar{\Gamma}\bar{\phi}_{\bar{x}} - \Lambda\bar{\phi}_{\bar{x}}^2 + o(\bar{\phi}_{\bar{x}}^2, M_\infty^2 - 1).$$

If we now retain only the lowest-order contributions to each term in (2.7) we find that the potential equation may be approximated by

$$(M_\infty^2 - 1 + 2\bar{\Gamma}\bar{\phi}_{\bar{x}} - \Lambda\bar{\phi}_{\bar{x}}^2)\bar{\phi}_{\bar{x}\bar{x}} + 2\bar{\phi}_{\bar{y}}\bar{\phi}_{\bar{x}\bar{y}} \approx \bar{\phi}_{\bar{y}\bar{y}}. \tag{3.14}$$

If we make use of (3.10), we find that the nonlinear term

$$\bar{\phi}_{\bar{y}}\bar{\phi}_{\bar{x}\bar{y}} = O\left[\left(1 - M_\infty^2\right)\bar{\phi}_{\bar{x}}\bar{\phi}_{\bar{x}\bar{x}}\right] = o(\bar{\phi}_{\bar{y}\bar{y}}),$$

from which we conclude it may be neglected relative to the $\bar{\phi}_{\bar{y}\bar{y}}$ term. Because of our assumption (1.10), we conclude that the nonlinear terms in the coefficient of $\bar{\phi}_{\bar{x}\bar{x}}$ in (3.14) are both of order $\bar{\phi}_{\bar{x}}^2 = O(\bar{\rho}^2)$ and one cannot be neglected or retained without the other. We now make the reasonable assumption that the nonlinear terms arising from those in the coefficient of $\bar{\phi}_{\bar{x}\bar{x}}$ are in balance with the linear terms appearing in (3.14). If the nonlinear terms were negligible, then (3.14) reduces to the linear wave equation and there would be no mechanism for the change in wave type characteristic of transonic flow. If the nonlinear terms dominate, the $\bar{\phi}_{\bar{y}\bar{y}} = O((1 - M_\infty^2)\bar{\phi}_{\bar{x}\bar{x}})$ term must be neglected and the governing equation involves only derivatives with respect to $\bar{x}$. As a result, the boundary conditions at the wing and infinity cannot be satisfied simultaneously. Thus,

$$\bar{\phi}_{\bar{x}} = O(\bar{\rho}) = O(\bar{\Gamma}) = O(|1 - M_\infty^2|^{\frac{1}{2}}) = o(1) \tag{3.15}$$

and, from (3.10),

$$\bar{\phi}_{\bar{y}} = O(1 - M_\infty^2) = o(1), \tag{3.16}$$

and the exact boundary value problem (2.7)–(2.9) may be approximated by

$$(M_\infty^2 - 1 + 2\bar{\Gamma}\bar{\phi}_{\bar{x}} - \Lambda\bar{\phi}_{\bar{x}}^2)\bar{\phi}_{\bar{x}\bar{x}} \approx \bar{\phi}_{\bar{y}\bar{y}}, \tag{3.17}$$

$$\bar{\phi}_{\bar{y}} \approx \epsilon F^{\pm\prime}, \quad \text{on} \quad \bar{y} \approx 0 \quad \text{for} \quad -\tfrac{1}{2} \leqslant \bar{x} \leqslant \tfrac{1}{2}, \tag{3.18}$$

$$\bar{\phi}_{\bar{x}}, \bar{\phi}_{\bar{y}} \to 0 \quad \text{as} \quad \bar{x}^2 + \bar{y}^2 \to \infty. \tag{3.19}$$

In (3.18) we have employed the usual thin-wing approximation

$$\bar{\phi}_{\bar{y}}(\bar{x}, \epsilon F^{\pm\prime}) \approx \bar{\phi}_{\bar{y}}(\bar{x}, 0).$$

Once (3.17)–(3.19) are solved, $\bar{\phi}(\bar{x}, \bar{y})$ may be employed to compute the pressure coefficient

$$c_p \equiv \frac{p - p_\infty}{\frac{1}{2}\rho_\infty U_\infty^2} \approx 2\bar{\rho} \approx -2\bar{\phi}_{\bar{x}}, \tag{3.20}$$

where a straightforward Taylor series for $p = p(\rho, s)$ and (3.11) have been employed.

The size of the density, pressure, and velocity perturbations relative to the thickness parameter may be determined by combining (3.16) with (3.18). Thus, $1-M_\infty^2 = O(\epsilon)$, and the size of each physical quantity may be summarized as follows

$$\frac{\rho_\infty \Gamma_\infty}{a_\infty}, \frac{\rho-\rho_\infty}{\rho_\infty}, c_p, \bar{\phi}_{\bar{x}} = O(\epsilon^{\frac{1}{3}}), \tag{3.21a}$$

$$|M_\infty^2 - 1|, \bar{\phi}_{\bar{y}} = O(\epsilon). \tag{3.21b}$$

That is, when (1.10) holds, the nonlinear terms seen in (3.17) are no longer negligible only when $|M_\infty^2 - 1| = O(\epsilon)$. Because $\bar{\Gamma} = o(1)$, the term $\bar{\Gamma}\bar{\phi}_{\bar{x}}$ in (3.17) is $\ll \bar{\phi}_{\bar{x}}$, higher-order nonlinear terms correctly neglected in the $\bar{\Gamma} = O(1)$ theory are of the same size as $\bar{\Gamma}\bar{\phi}_{\bar{x}}$. The preceding analysis demonstrates that the only additional term is the quadratic term $\Lambda\bar{\phi}_{\bar{x}}^2$ seen in (3.17).

As discussed in §1, the relatively weak nonlinearity of the small-$\bar{\Gamma}$ case results in a delay of the onset of the nonlinear effects characteristic of transonic flow. That is, the transonic range is narrowed when the intrinsic nonlinearity is weak. This is particularly evident when we compare the results summarized in (3.21) to those of the $\bar{\Gamma} = O(1)$, i.e. classical, theory where both c_p and $|M_\infty^2 - 1|$ are of order $\epsilon^{\frac{2}{3}}$. The transonic range of the present theory is seen to be an order of $\epsilon^{\frac{1}{3}}$ smaller than that of the classical theory. The resultant pressure coefficient is an order $\epsilon^{-\frac{1}{6}}$ larger than that of the classical theory. We would naturally expect this effect to lead a comparable increase in the lift found in subcritical flows.

The increase of the size of c_p is to be expected in the light of the decrease in the extent of the transonic regime. In essence, this increase is due to the Prandtl–Glauert singularity. For example, we could have anticipated this result by consideration of the well-known Prandtl–Glauert scaling law

$$c_p = \frac{c_{p\text{inc}}}{(1-M_\infty^2)^{\frac{1}{2}}}, \tag{3.22}$$

where c_p is the pressure coefficient at M_∞ and $c_{p\text{inc}}$ is the incompressible ($M_\infty = 0$) coefficient. If we take $c_{p\text{inc}} = O(\epsilon)$ and employ (3.21*b*), we find that (3.22) yields

$$c_p = O(\epsilon^{\frac{1}{3}}),$$

which is in complete accord with (3.21*a*).

A second route to the determination of the boundary-value problem (3.17)–(3.19) is through use of the well-known method of matched asymptotic expansions; see e.g. Kevorkian & Cole (1981) or Cole & Cook (1986). Here the small-disturbance parameter would be taken to be ϵ. Condition (1.10) is then enforced by taking $\epsilon \to 0$ with $\bar{\Gamma}\epsilon^{-\frac{1}{2}}$ fixed. When this more systematic approach is employed, it is found to be in complete agreement with results presented here.

We conclude this section with a few remarks concerning the nonlinearity parameters $\bar{\Gamma}$ and Λ. Formulae suitable for the calculation of $\bar{\Gamma}$ from p, V, T data have been given by Bethe (1946), Lambrakis & Thompson (1972), and Cramer (1989*a*). Analogous formulae for the calculation of Λ are given by Cramer (1987). Because Λ is just a non-dimensional version of the slope of the Γ *vs.* ρ curve, it is necessarily positive near the high-density zero of Γ and is necessarily negative near the low-density zero. Although $\bar{\Gamma}$ must be evaluated at the actual free-stream state, Λ may be approximated by its value at the $\Gamma = 0$ point with no loss in accuracy. That is, Λ may be computed from the slope of the Γ *vs.* ρ curve evaluated exactly at $\Gamma = 0$. If we confine our attention to a single isentrope in the neighbourhood of one

Fluid	Formula	T (K)	p (atm)	Λ
pf-tributylamine (FC-43)	$C_{12}F_{27}N$	566.5	10.9	2.3
		562.9	10.0	−1.0
pf-tripentylamine (FC-70)	$C_{15}F_{33}N$	609.5	10.1	2.9
		606.2	9.2	−1.1
pf-trihexylamine (FC-71)	$C_{18}F_{39}N$	649.1	9.4	2.7
		646.3	8.5	−1.2
pf-perhydrofluorene (PP10)	$C_{13}F_{22}$	631.4	15.7	3.0
		626.1	14.1	−1.2
pf-perhydrophenanthrene (PP11)	$C_{14}F_{24}$	651.7	14.4	2.6
		647.5	13.0	−1.1
pf-fluoranthene (PP24)	$C_{16}F_{26}$	704.9	15.3	3.5
		700.5	13.7	−1.3
pf-benzyltetralin (PP25)	$C_{17}F_{30}$	681.9	11.0	1.3
		678.9	10.2	−0.8

TABLE 1. Computed values of Λ for various fluids. The manufacturer's designation is given in parentheses after the chemical name. For each fluid, the upper thermodynamic state corresponds to a high-pressure zero of Γ. The lower state is the low-pressure zero on the same isentrope.

zero or the other, we may regard Λ as fixed, while $\bar{\Gamma}$ may be varied by choosing different states along the isentrope. The fact that $\bar{\Gamma}$ and Λ may be varied independently will be employed in the following sections.

Numerical estimates for Λ may be obtained through use of the general formulae given by Cramer (1987) or by numerical approximation of the derivative in (3.6). In the present study we take the latter approach. We first computed Γ along an isentrope by the scheme already employed by Cramer & Best (1991). If a zero in Γ was encountered, a simple centred-difference approximation was employed to estimate Λ. The difference formula was centred about the zero so that the value of Λ is that at $\Gamma = 0$. The equation of state is the Martin–Hou (1955) equation with a power-law specific heat at constant volume. The fluids chosen are a selection of commercially available fluorocarbons currently employed in heat transfer applications. For a more detailed account of the fluid properties and implementation of the Martin–Hou equation, we refer the reader to the articles by Cramer (1989*a*) and Cramer & Best (1991).

Typical values of the pressure, temperature, and values of Λ at zeros of Γ are recorded in table 1. For each fluid two states are given, corresponding to high- and low-pressure zeros on the same isentrope. In each case, the isentrope chosen is that passing through the point $V = 0.7V_c$, $T = 1.02T_c$, where $V \equiv \rho^{-1}$ is the specific volume and the subscript c denotes values at the thermodynamic critical point of the fluid. Calculations with other fluids and other thermodynamic states show that the results given here are typical in that the value of Λ at the high-pressure zero ranges from about 1 to 4 and from -0.5 to -2.5 near the low-pressure zero.

Finally, we note that the local value of $\bar{\Gamma}$ varies from point to point in the flow. In the context of the present theory, we approximate this quantity as follows:

$$\bar{\Gamma}_1(\bar{\rho}) \approx \bar{\Gamma} + \Lambda\bar{\rho} + o(\bar{\rho}) \approx \bar{\Gamma} + \tfrac{1}{2}\Lambda c_p + o(c_p), \tag{3.23}$$

where (3.20) has been employed.

4. Similitude

Analytical solutions to (3.17)–(3.19), easily applied to configurations of practical interest, are currently not available. It will therefore be useful to determine any similarity parameters for these flows. Here we will apply the following scalings to $\bar{\phi}$, $\bar{x}, \bar{y}$:

$$\bar{\phi} = \frac{\epsilon^{\frac{2}{3}}}{\bar{\Gamma}^{\frac{1}{3}}}\psi, \quad \bar{x} = \xi, \quad \bar{y} = \frac{\eta}{\epsilon^{\frac{1}{3}}|\bar{\Gamma}|^{\frac{1}{3}}}, \tag{4.1}$$

where ψ, ξ, η are order-one scaled variables. The use of the absolute value of $\bar{\Gamma}$ in the scalings for $\bar{y}$ ensures that $\eta > 0$ whenever $\bar{y} > 0$. If (4.1) are substituted in (3.17)–(3.19) we find that $\psi(\xi, \eta)$ is governed by

$$(-K_1 + 2\psi_\xi - K_2\psi_\xi^2)\psi_{\xi\xi} = \psi_{\eta\eta}, \tag{4.2}$$

$$\psi_\eta = \operatorname{sgn}(\bar{\Gamma})F^{\pm\prime}(\xi) \quad \text{on} \quad \eta = 0, \tag{4.3}$$

$$\psi_\xi, \psi_\eta \to 0 \quad \text{far from the blade}, \tag{4.4}$$

where

$$K_1 \equiv (1 - M_\infty^2)/(\epsilon\bar{\Gamma})^{\frac{2}{3}}, \tag{4.5}$$

$$K_2 \equiv \Lambda\epsilon^{\frac{2}{3}}/\bar{\Gamma}^{\frac{4}{3}}, \tag{4.6}$$

and sgn $(\bar{\Gamma})$ denotes the sign of $\bar{\Gamma}$. The quantity K_1 is recognized as a form of the usual transonic similarity parameter. The quantity K_2 is a second parameter arising from the presence of the second nonlinear term in (3.17). The form (4.2)–(4.6) is particularly convenient because it reduces to the classical result when $\bar{\Gamma} = O(1)$. In that case, $K_2 = O(\epsilon^{\frac{2}{3}})$ and the second nonlinear term in (4.2) may be neglected. The condition for $K_1 = O(1)$ is then the classical one, i.e. $|1 - M_\infty^2| = O(\epsilon^{\frac{2}{3}})$.

When (4.1) are applied to (3.20), the pressure coefficient is found to be

$$c_p = -2(\epsilon^{\frac{2}{3}}/\bar{\Gamma}^{\frac{1}{3}})\psi_\xi, \tag{4.7}$$

or, if we define

$$\tilde{c}_p \equiv -2\psi_\xi = O(1), \tag{4.8}$$

we have

$$c_p = (\epsilon^{\frac{2}{3}}/\bar{\Gamma}^{\frac{1}{3}})\tilde{c}_p. \tag{4.9}$$

By combining (4.9) with (3.23) we also find that the local value of $\bar{\Gamma}$ may be written

$$\bar{\Gamma}_1 = \bar{\Gamma}(1 + \tfrac{1}{2}K_2\tilde{c}_p). \tag{4.10}$$

Our scaled equations (4.2)–(4.4) indicate that two flows over the same wing or blade profile are self-similar if the sign of $\bar{\Gamma}$ is the same for each flow and the similarity parameters K_1 and K_2 have the same value in each flow. From the form of the above boundary-value problem and the definition (4.6) it is immediately obvious that similarity may be obtained only if $\bar{\Gamma}$ and Λ are of the same sign in each flow. That is, a change in sign either of $\bar{\Gamma}$ or Λ gives rise to qualitative changes in the general flow pattern. The fact that $\bar{\Gamma} > 0$ and $\bar{\Gamma} < 0$ flows are qualitatively different is to be expected. We may motivate the observation that $\Lambda > 0$ and $\Lambda < 0$ flows are fundamentally different by considering a $\bar{\Gamma} > 0$ flow with $\Lambda < 0$. From (3.23) or (4.10) we see that the local value of $\bar{\Gamma}$ in regions of expansion, i.e. $c_p < 0$, will remain positive. However, if $\Lambda > 0$ such regions may result in $\bar{\Gamma}_1 > 0$, thus giving rise to fundamentally different nonlinearity.

Another advantage of the scalings used here is that the effect of changing the sign of $\bar{\Gamma}$ is immediately clear. Because K_1 and K_2 are invariant with respect to such sign changes, a change in sign of $\bar{\Gamma}$ is equivalent to replacing the wing shape $F^{\pm}(x)$ by $-F^{\pm}(\bar{x})$. That is, a hump (dip) in a $\bar{\Gamma} < 0$ flow is similar to a $\bar{\Gamma} > 0$ flow over a dip (hump), provided K_1 and K_2 have been matched. As an example, we note that we may use our intuition pertaining to $\bar{\Gamma} > 0$ and $\Lambda = 0$ flows to immediately deduce the flow when $\bar{\Gamma} < 0$, $\Lambda = 0$. In particular, the well-known fact that a $\bar{\Gamma} > 0$, $\Lambda = 0$ flow over a dip is entirely subsonic and therefore shock-free may be used to conclude that a $\bar{\Gamma} < 0$, $\Lambda = 0$ flow over a hump, i.e. airfoil configuration, will also be entirely subsonic and shock-free.

In the theory of perfect gases, $\bar{\Gamma} > 0$, Λ is ignored, and the critical Mach number is characterized by a single number K_{1c} which is just the value of K_1 at the critical Mach number. In the present theory, the occurrence of the second and third similarity parameters means that

$$K_{1c} = K_{1c}(K_2, \operatorname{sgn} \bar{\Gamma}),$$

which is recognized as significantly more complicated than the condition of the classical theory.

5. Mach number variation

In this section, we analyse the variation of the Mach number with density or pressure as predicted by (3.17)–(3.19) or (4.2)–(4.4). To begin we consider the square of the particle velocity expressed in terms of the disturbance potential $\bar{\phi}$ given in (2.6). It is easily verified that this reads

$$v^2 = U_\infty^2 \{1 + 2\bar{\phi}_{\bar{x}} + \bar{\phi}_{\bar{x}}^2 + \bar{\phi}_{\bar{y}}^2\},$$

exactly. The Mach number $M = v/a$ may therefore be written

$$M^2 = M_\infty^2 \{1 + 2\bar{\phi}_{\bar{x}} + \bar{\phi}_{\bar{x}}^2 + \bar{\phi}_{\bar{y}}^2\}/\bar{a}^2. \tag{5.1}$$

If we employ (3.13), we find

$$\bar{a}^{-2} = 1 - 2\bar{\phi}_{\bar{x}} + 2\bar{\Gamma}\bar{\phi}_{\bar{x}} + (3 - \Lambda)\bar{\phi}_{\bar{x}}^2 + o(\bar{\phi}_{\bar{x}}^2),$$

which, when combined with (5.1) yields

$$M^2 = M_\infty^2 \{1 + 2\bar{\Gamma}\bar{\phi}_{\bar{x}} - \Lambda\bar{\phi}_{\bar{x}}^2 + o(\bar{\phi}_{\bar{x}}^2)\},$$

where the fact that $\bar{\phi}_{\bar{y}} \ll \bar{\phi}_{\bar{x}}$ has been employed. Thus, the local value of M may be expressed:

$$M^2 - 1 = M_\infty^2 - 1 + 2\bar{\Gamma}\phi_{\bar{x}} - \Lambda\bar{\phi}_{\bar{x}}^2 + o(\bar{\phi}_{\bar{x}}^2, M_\infty^2 - 1), \tag{5.2}$$

which, when combined with (3.17), yields a third form of the governing boundary-value problem:

$$(M^2 - 1)\bar{\phi}_{\bar{x}\bar{x}} = \bar{\phi}_{\bar{y}\bar{y}}, \tag{5.3}$$

$$\bar{\phi}_{\bar{y}} = \epsilon F^{\pm\prime}(\bar{x}) \quad \text{on} \quad \bar{y} \approx 0 \quad \text{for} \quad -\tfrac{1}{2} \leqslant \bar{x} \leqslant \tfrac{1}{2} \tag{5.4}$$

$$\bar{\phi}_{\bar{x}}, \bar{\phi}_{\bar{y}} \to 0 \quad \text{far from the wing}, \tag{5.5}$$

where (5.4) and (5.5) are identical to (3.18) and (3.19) but repeated here for completeness. As in the classical theory, (3.17) and (5.3) change type as the local value of $M^2 - 1$ changes sign.

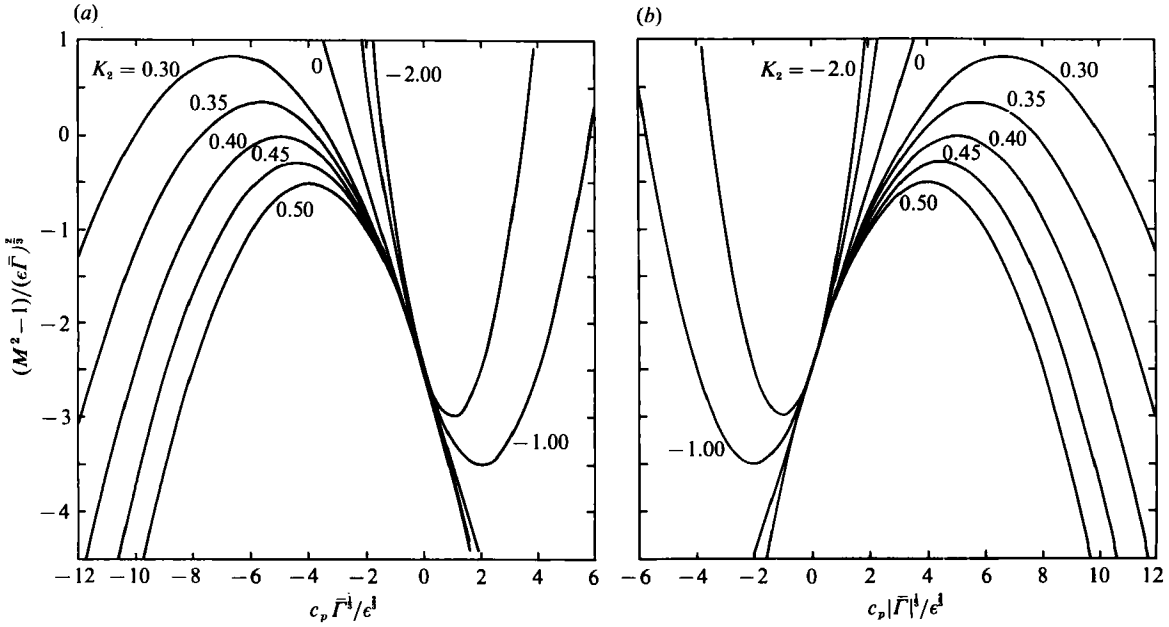

FIGURE 5. Plot of scaled Mach number variation with the scaled pressure coefficients according to (5.4). Here $K_1 = 2.5$ and (*a*) $\bar{\Gamma} > 0$, (*b*) $\bar{\Gamma} < 0$.

The variation of the Mach number with pressure is found if (3.20) is employed to replace $\bar{\phi}_{\bar{x}}$ by c_p in (5.2). If, in addition, the scalings (4.1) and (4.9) are employed, we find that (5.2) may be rewritten as

$$(M^2-1)/(\epsilon\bar{\Gamma})^{\frac{2}{3}} = -K_1 - \tilde{c}_p - \tfrac{1}{4}K_2\tilde{c}_p^2. \tag{5.6}$$

A plot of M^2-1 *vs.* $\tilde{c}_p$ has been provided in figure 5 for the case $K_1 = 2.5$ and various values of K_2. Because the sign of $\tilde{c}_p$ depends on the sign of $\bar{\Gamma}$, separate plots of the $\bar{\Gamma} > 0$ and $\bar{\Gamma} < 0$ cases have been made. Each curve is recognized as a parabola. If (5.3) is differentiated, it is easily demonstrated that

$$\frac{\mathrm{d}}{\mathrm{d}\tilde{c}_p}\left(\frac{M^2-1}{(\epsilon\bar{\Gamma})^{\frac{2}{3}}}\right) = -(1+\tfrac{1}{2}K_2\tilde{c}_p) \tag{5.7}$$

$$= -\bar{\Gamma}_1/\bar{\Gamma}, \tag{5.8}$$

where (4.10) has been employed. Thus, the maximum or minimum of each parabola occurs at

$$\tilde{c}_{pm} = -\frac{2}{K_2} \quad \text{or, equivalently,} \quad \bar{\Gamma}_1 = 0. \tag{5.9}$$

The fact that the extrema of M occur where the local value of Γ changes sign has also been found in the analysis of the dissipative, albeit nearly isentropic, structure of shock waves in BZT fluids.

To illustrate the relation between the present small-disturbance theory and the exact isentropic theory we have sketched the Mach number variation of both models in figure 6. In each case, the curves based on the small-disturbance theory correspond

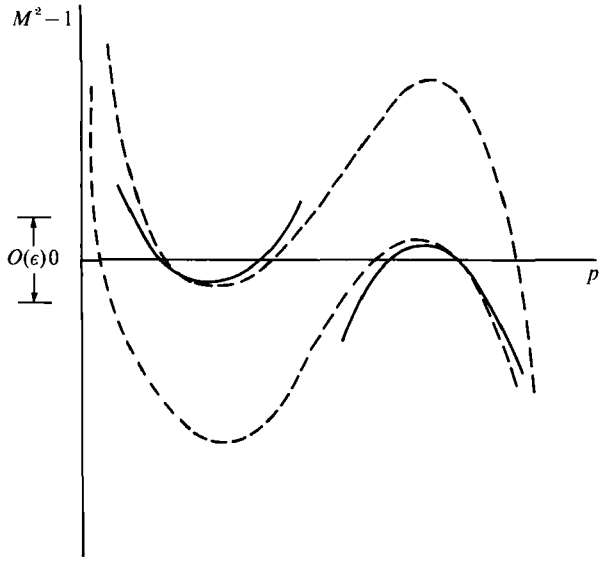

FIGURE 6. Comparison of the exact and approximate Mach number variations. The dashed line denotes the exact M *vs.* p relation and the solid line denotes that employed in the present investigation.

to $\bar{\Gamma} > 0$. It is seen that the $K_2 < 0$ branches in figure 5 correspond to the local minimum in M seen in figure 3. The $K_2 > 0$ branch corresponds to the local maximum.

The Mach number variation used in the present investigation is seen to be completely consistent with the exact variation, provided the small-disturbance assumption is satisfied. If, in a particular flow, this assumption is violated, the present theory may not yield results which are in qualitative agreement with the actual dynamics. Inspection of figure 6 shows that compressions large enough to violate the small-disturbance approximation give rise to qualitatively incorrect behaviour when $K_2 < 0$. Large expansions also yield qualitatively incorrect results when $K_2 > 0$. This contrasts with the perfect gas theory where the qualitative behaviour is, for the most part, correct even when the small-disturbance approximation breaks down.

The most common failure of the small-disturbance approximation is at blunt or pointed leading edges and at pointed trailing edges of conventional turbine blade or wing configurations. At such points c_p becomes of order one and positive. In this case, we expect that the flow details in the region of large c_p will not be representative if $K_2 < 0$. From figure 6 it should be clear that the Mach number will initially increase, and may even exceed one, as the pressure increases. However, the Mach number will ultimately decrease once c_p becomes of order one. This initial increase followed by a decrease is qualitatively similar to the $K_2 > 0$ branch although the free-stream Mach number or, equivalently, the stagnation pressure, differs for each branch. Because we expect the regions of large c_p to be small, we would naturally expect the region of disagreement between the present and exact theories to be localized as well. To test these and other difficulties, the present authors have developed a higher-order theory analogous to the extended perturbation scheme found in §5 of the article by Cramer & Crickenberger (1991). The results of that study will be reported in future publications.

6. Estimates for the critical Mach number

In any transonic flow, sonic points and the critical Mach number M_c play a central role. In the classical theory, one and only one sonic point can be attained in a continuous expansion or compression. If $\bar{\Gamma} > 0$, then sufficiently strong expansions give rise to supersonic flow whereas compressions may result in supersonic flow if $\bar{\Gamma} < 0$. In the non-classical ($\Lambda \neq 0$) theory, either two sonic points or none are possible. If we set the local Mach number equal to one in (5.6) and solve the resultant quadratic for $\tilde{c}_p$, we find that the sonic points are given by

$$\tilde{c}_{p\text{sonic}} = (2/K_2)\{-1 \pm (1-K_1K_2)^{\frac{1}{2}}\}. \tag{6.1}$$

Sonic points therefore exist only if

$$K_1K_2 = \Lambda(1-M_\infty^2)/\bar{\Gamma}^2 < 1, \tag{6.2}$$

where (4.5)–(4.6) have been employed. In this section, we first consider only flows having subsonic free streams. At the low-density zero of Γ, $\Lambda < 0$ and (6.2) is therefore always satisfied. This case corresponds to the $K_2 < 0$ curves found in figure 5. In this case, the number of sonic points which will be observed in a particular flow will depend on the size of the disturbance generated by the wing or blade. Here we note that both compressions ($c_p > 0$) and expansions ($c_p < 0$) may give rise to supersonic flow. In both the $\Gamma < 0$ and $\Gamma > 0$ cases, it appears that sonic conditions are obtained at smaller values of $|c_p|$ than in the classical case. In this case, it seems likely that the critical Mach number will be decreased by the non-classical effects, at least for a fixed value of $\bar{\Gamma}$.

Near the large-density zero of Γ, $\Lambda > 0$ and the condition (6.2) may or may not be satisfied, depending on the size of $1-M_\infty^2$. In particular, the flow remains entirely subsonic, regardless of the size of the disturbance, if

$$M_\infty < (1-(\bar{\Gamma}^2/\Lambda))^{\frac{1}{2}} \approx 1-\tfrac{1}{2}\bar{\Gamma}^2/\Lambda. \tag{6.3}$$

This conclusion is in marked contrast with the classical ($\Lambda = 0$) theory where increases in the strength of the disturbance will ultimately always drive the flow supersonic. It can also be noted that the criterion (6.3) only depends on the thermodynamic state of the free stream. Thus, knowledge of the free stream immediately yields a sufficient condition on the Mach number for the generation of a subcritical flow without regard for the wing shape.

We now provide numerical estimates for the critical Mach number. In the remainder of this section, we restrict our attention to the case where $\bar{\Gamma} > 0$, $\Lambda > 0$. This case is of particular interest because it is most likely to give rise to the maximum critical Mach number. For the purposes of demonstration, we take the general measure of the disturbance and the free-stream thermodynamic state to be fixed. Thus, ϵ, $\bar{\Gamma}$, Λ, and K_2 may be regarded as fixed.

In the following we will employ the Prandtl–Glauert scaling (3.22) in order to account for the specific blade characteristics. This scaling law is, of course, based on the linear theory and only provides an approximation to the actual pressure distribution at critical conditions. However, it is widely employed in the perfect gas theory, see e.g. Anderson (1990), and will therefore provide a convenient method of illustrating the differences between BZT fluids and lighter substances. With this in mind, we will write the minimum value of $\tilde{c}_p$ as

$$\tilde{c}_{p\min} = c_{p0}/(\epsilon K_1^{\frac{1}{2}}). \tag{6.4}$$

Here the quantity c_{p0} is the minimum value of c_p for the same blade, albeit in an incompressible flow. Because the incompressible flow is governed by linear equations, c_{p0}/ϵ is a pure number characteristic of the specific wing or blade shape.

It is expected that the flows will begin at the free-stream condition, and undergo a compression ($c_p > 0$) as the leading edge of the blade or wing is approached. The flow then expands ($c_p < 0$) over the top of the blade or wing. This, of course, is similar to the behaviour of perfect gases. Inspection of figure 5(*a*) reveals that it is in this expansion region where the supersonic flow will be generated, at least in the example discussed here, i.e. $\bar{\Gamma} > 0$, $\Lambda > 0$. We therefore conclude that the sonic point of interest is the larger of the two roots in (6.1), i.e.

$$\tilde{c}_{p\text{sonic}} = (2/K_2)\{-1 + (1 - K_1 K_2)^{\frac{1}{2}}\}. \tag{6.5}$$

Straightforward differentiation of (6.5) reveals that $\tilde{c}_{p\text{sonic}}$ decreases monotonically as K_1 increases. We therefore obtain the expected result that the strength of the expansion required to accelerate the flow to a supersonic state must increase as M_∞ decreases from one.

It can be shown that two cases are of interest. The first holds for relatively small K_2 and, as one expects, yields a criterion similar to that of the classical theory. At sufficiently small values of M_∞, inspection of (6.4)–(6.5) reveals that $\tilde{c}_{p\min} > \tilde{c}_{p\text{sonic}}$, or because $\tilde{c}_p < 0$,

$$|\tilde{c}_{p\min}| < |\tilde{c}_{p\text{sonic}}|.$$

As M_∞ is increased, K_1 will decrease, thus resulting in a monotonic increase in $|\tilde{c}_{p\min}|$ and a monotonic decrease in $|\tilde{c}_{p\text{sonic}}|$. Ultimately,

$$|\tilde{c}_{p\text{sonic}}| < |\tilde{c}_{p\min}|.$$

If we assume that the local value of M decreases with increasing $\tilde{c}_p$, the above condition necessarily implies that the flow is supersonic. As in the classical theory, the criterion for the critical Mach number will then be

$$\tilde{c}_{p\text{sonic}}(K_1, K_2) = \tilde{c}_{p\min} = \frac{c_{p0}}{\epsilon K_1^{\frac{2}{3}}}. \tag{6.6}$$

The critical Mach number is found by solving (6.6) iteratively for K_1 with K_2 fixed. It is easily demonstrated that one and only one root of (6.6) exists provided

$$0 \leqslant K_2 \leqslant K_{2\text{crit}} \tag{6.7}$$

where

$$K_{2\text{crit}} \equiv (-2\epsilon/c_{p0})^{\frac{2}{3}}. \tag{6.8}$$

Later in this section it will be shown that (6.6) is no longer the correct criterion when (6.7) is violated.

To contrast this case with that corresponding to larger values of K_2, we have plotted the Mach number variation with $\tilde{c}_p$ for various values of K_1 and a fixed K_2 in figure 7(*a*). In the case shown, $K_2 = \frac{1}{2}$ and $c_{p0} = -4.5\epsilon$. The value of c_{p0} is in the general neighbourhood of that of a circular-arc airfoil with half-thickness ϵ. The values of $\tilde{c}_{p\min}$, as computed by (6.4), are denoted by circles. Inspection of figure 7 reveals that the critical value of K_1, hereinafter denoted by K_{1c}, is between 1.5 and 2.0. This observation is in complete agreement with iteration of (6.6), the result of which yields $K_{1c} \approx 1.93$.

The key assumption leading to the criterion (6.6) is that the Mach number must be a decreasing function of $\tilde{c}_p$, particularly near the point where $\tilde{c}_{p\min} = \tilde{c}_{p\text{sonic}}$. An

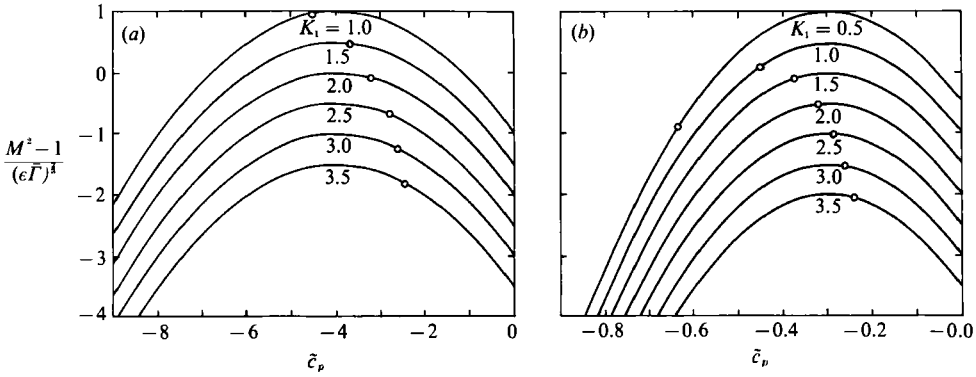

FIGURE 7. Plots of Mach number *vs.* $\tilde{c}_p$ for (*a*) $K_2 = \frac{1}{2}$ and (*b*) $K_2 = \frac{2}{3}$, and $\bar{\Gamma} > 0$. The open circles denote the minimum value of the pressure coefficient if the minimum c_p in an incompressible flow is -4.5ϵ, as computed from (6.4).

example of the failure of this assumption is seen in figure 7(*b*) where the Mach number variation with $\tilde{c}_p$ is plotted for various values of K_1 and $K_2 = \frac{2}{3}$, $c_{p0} = -4.5\epsilon$. The wing or blade is recognized as identical to that of figure 7(*a*) but K_2 is slightly larger. In figure 7(*b*) it is seen that $\tilde{c}_{p\min}$ becomes less than the $\tilde{c}_p$ corresponding to the local maximum in the Mach number when K_1 is between 2.0 and 2.5. The precise value of K_1 at which this occurs can be computed by equating the expression (6.4) for $\tilde{c}_{p\min}$ to the expression (5.9) for the $\tilde{c}_p$ at which the local Mach number has an extremum. After minor rearrangement and use of the definition (6.8), the resultant expression reads

$$K_1 = K_2^2/(K_{2\text{crit}})^3. \tag{6.9}$$

If we substitute our value of c_{p0} in (6.8), we find that $K_{2\text{crit}} \approx 0.582$ and that $\tilde{c}_{p\min} > -2/K_2$ if and only if $K_1 > 2.25$. This is in complete agreement with the results depicted in figure 7(*b*) where the transition is seen to occur at a point between 2.0 and 2.5.

In the example just discussed, the minimum-pressure point lies to the left of the local maximum in M and it is clear that part of the flow can become supersonic while the minimum-pressure point still corresponds to subsonic flow. As a result, condition (6.6) is no longer appropriate. When this is the case, the sonic points first occur when the maximum Mach number becomes equal to one. Thus, the appropriate criterion is

$$K_{1c} = 1/K_2. \tag{6.10}$$

The precise condition under which (6.10) must replace (6.6) is obtained by requiring that

$$\tilde{c}_{p\min} < -2/K_2$$

at $K_1 = K_2^{-1}$. If we make use of (6.4) and (6.8) and rearrange, we find that (6.10) holds whenever

$$K_2 > K_{2\text{crit}}. \tag{6.11}$$

Finally, we note that the critical Mach number corresponding to (6.10) is

$$M_c = (1-(\bar{\Gamma}^2/\Lambda))^{\frac{1}{2}} \approx 1-\tfrac{1}{2}\bar{\Gamma}^2/\Lambda, \tag{6.12}$$

which is, of course, similar to (6.3).

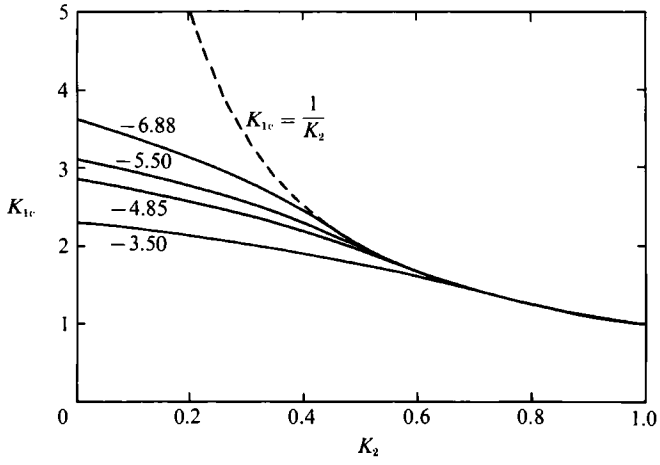

FIGURE 8. Computed values of the critical K_1 for blades having $c_{p0}/\epsilon \approx -3.50$, -4.85, -5.50, and -6.88, where c_{p0} is the minimum pressure coefficient in an incompressible flow over the same blade. The second and fourth values correspond to a circular-arc airfoil and a NACA 00XX of half-thickness ϵ at zero angle of attack.

At this stage two observations can be made. The first is that the critical Mach number becomes independent of the geometry of the wing or blade when (6.11) is satisfied. A more significant point with respect to applications is that $M_c \to 1$ as $\bar{\Gamma} \to 0$. Thus, it appears that subcritical flow may be maintained up to arbitrarily large values of M_∞ (< 1) simply by adjusting the thermodynamic state of the free stream arbitrarily close to a $\Gamma = 0$ point.

The conclusion that $M_c \to 1$ as $\bar{\Gamma} \to 0$ is based on the assumption that (6.11) holds. It is easily demonstrated that the same limit, i.e. $\bar{\Gamma} \to 0$, will always result in (6.11) being satisfied. If, for example, we fix the blade shape and consider a sequence of states on a particular isentrope, then $K_{2\text{crit}}$, ϵ, and A can be regarded as fixed. Inspection of (4.6) shows that K_2 will increase monotonically as $\bar{\Gamma} \to 0$. Because $K_{2\text{crit}}$ is fixed (6.11) will ultimately be satisfied regardless of the initial state.

To illustrate the variation of K_{1c} we have plotted this quantity versus K_2 in figure 8. The only input required is the parameter c_{p0}/ϵ which characterizes the blade shape. The largest value of $|c_{p0}/\epsilon|$ was computed from data for a NACA 0012 airfoil at 0° angle of attack and, within the context of a small-disturbance theory, should be applicable to any of the airfoils in the NACA 00XX series. The value of $c_{p0} \approx -4.85\epsilon$ was computed from data for a circular-arc airfoil of half-thickness ϵ. For reference we have also included the $K_{1c} = K_2^{-1}$ curve as a dashed line. As expected, solutions to (6.6) depend on the details of the wing or blade shape. Non-similar blades will therefore have different values of K_{1c} and the critical Mach number M_c. However, once condition (6.11) is attained, the critical similarity parameter and critical Mach number no longer depend on the details of the wing or blade. In figure 8, this is seen as the ultimate coalescence of the curves with the $K_{1c} = K_2^{-1}$ curve. From (6.12) we may also observe that the critical Mach number will only depend on the thermodynamic state of the free stream when $K_2 > K_{2\text{crit}}$.

As an illustration of the possible increases in the critical Mach number of BZT fluids, we have estimated M_c for the flow of air, steam, and PP11 over a NACA 0012 airfoil at 0° angle of attack. Thus, we have taken $c_{p0} \approx -0.41$ and $\epsilon = 0.06$. The free-stream temperature was taken to be 653 K which is slightly above the critical temperatures of steam and PP11. For the present purposes, the perfect gas model

Fluid	T_∞ (K)	p_∞ (atm)	$\rho_\infty \Gamma_\infty / a_\infty$	Λ	K_{1c}	M_c
Air	653	low	1.20	0	3.6	0.61
Steam	653	low	1.15	0	3.6	0.63
PP11	653	14.6	0.25	0	3.6	0.88
PP11	653	14.6	0.25	2.6	0.4	0.988

TABLE 2. Comparison of critical Mach numbers for a NACA 0012 airfoil. Values of $\rho_\infty \Gamma_\infty / a_\infty$ for air and steam were computed using (1.7) with the ratio of specific heats taken to be the value at 653 K. The value for PP11 was computed using the Martin–Hou (1955) equation of state.

will give a reasonable estimate of the value of $\bar{\Gamma}$ for air and steam. Because $\bar{\Gamma} = O(1)$ for both air and steam, the classical ($\Lambda = 0$) theory was employed to estimate the critical value of K_1. This yields

$$K_{1c} = (c_{p0}/\epsilon)^{\frac{2}{3}} \approx 3.6.$$

The thermodynamic state of the PP11 was taken to be along the same isentrope as used in table 1. As a result, we may take $\Lambda \approx 2.6$. The results are listed in table 2. Even in the classical theory, we expect M_c to increase if the intrinsic nonlinearity parameter $\rho\Gamma/a$ becomes small. The magnitude of this increase is seen by comparing the $\Lambda = 0$ calculation for PP11 to that for air and steam. However, when the correct value of Λ is employed even larger increases in M_c are observed. The critical Mach number for PP11 is seen to be over 50% larger than that for steam flowing at the same free-stream temperature over the same blade. Even more significant for applications is the increase in the Prandtl–Glauert factor $(1-M_c^2)^{-\frac{1}{2}}$. For PP11 this factor is found to be approximately five times larger than that for steam. If similar advantages carry over to lifting airfoils, and we have no reason to think that they will not, the lift coefficient appears to be increased by a factor of five simply by replacing steam by PP11. We note that these benefits occur with no increase in drag.

These predictions are, of course, based on the small-disturbance theory developed in the preceding sections. Inspection of figures 3 and 6 show that the qualitative variation of the Mach number is the same as that predicted here over a considerably wider range of densities. Thus, even if the small-disturbance assumption is violated, the upper bound on the local Mach number will result in critical Mach numbers approximately equal to those predicted here. However, inspection of the same figures reveals that the theoretical limit of $M_c = 1$ will never be achieved in real BZT fluids. The reason for this is that the amplification of the disturbance due to the large subsonic Mach numbers can drive the minimum pressure below that corresponding to the local minimum in M and ultimately below that corresponding to the low-pressure sonic point. Thus, the critical Mach number will always be limited to a value less than one. This conclusion is in complete accord with our intuition. The precise limit on the critical Mach number will require a more general model for the Mach number variation. However, a quick estimate of the effect of this limit can be obtained through use of the numerical scheme presented in the following sections. If we again consider a NACA 0012 airfoil with $\bar{\Gamma} = 0.25$, $\Lambda = 2.6$, we find that the minimum value of ρ is about $0.47\rho_c$ and the maximum value of M is approximately 0.96 when $M_\infty = 0.95$. If this minimum density is compared to the values along the exact isentrope, we find that the point of minimum pressure and density is just at the low-pressure zero of Γ. In turn, this should approximately correspond to the local

minimum in the Mach number seen in figures 3 and 6. Based on this crude calculation, it appears that the critical Mach number is still above 0.95. Further estimates of the same type suggest that $M_c \approx 0.96$ for this case. It should also be noted that tests with different fluids or airfoils having more slender cross-sections yield similar increases in the critical Mach number and the Prandtl–Glauert amplification factor. We therefore conclude that the general magnitude of the increases predicted by the present theory are reasonable; the determination of more precise values is left for future studies.

7. Numerical scheme

In order to obtain detailed solutions to systems (3.17)–(3.19) and (5.3)–(5.5) it is necessary to develop a numerical approximation scheme. In the present investigation we employ a version of the well-known method of Murman & Cole (1971); see also Murman (1973) and Fletcher (1988). For illustration, we restrict our attention to symmetric wings or blades at 0° angle of attack. Thus, only the half-plane problem will be considered in this preliminary investigation. The boundary-value problem will therefore be modelled by

$$(1-M_\infty^2-2\bar{\Gamma}\bar{\phi}_{\bar{x}}+\Lambda\bar{\phi}_{\bar{x}}^2)\,\bar{\phi}_{\bar{x}\bar{x}}+\bar{\phi}_{\bar{y}\bar{y}} = -\nu\bar{\phi}_{\bar{x}\bar{x}\bar{x}\bar{x}}, \tag{7.1}$$

$$\bar{\phi}_{\bar{y}} = \epsilon F'(\bar{x}) \quad \text{on} \quad \bar{y}=0, \tag{7.2}$$

$$\bar{\phi}_{\bar{y}} = 0 \quad \text{on} \quad y=h, \tag{7.3}$$

$$\bar{\phi}_{\bar{x}} = 0 \quad \text{on} \quad \bar{x} = \pm\tfrac{1}{2}W, \tag{7.4}$$

where (7.2)–(7.3) are recognized as the usual Neumann boundary conditions applied on a finite box of total width $W>0$ and height $h>0$. Here we will find it convenient to include an artificial viscosity term on the right-hand side of the basic differential equation. The quantity $\nu>0$ is the small artificial viscosity constant typically taken to have values between 10^{-4} and 10^{-3}.

The function $F'(\bar{x}) \equiv F^{+\prime}(\bar{x})$ is the scaled wall or wing slope. In the following section, we select $F(\bar{x})$ from the following two configurations. The first corresponds to a circular-arc airfoil, in which case we take

$$F(\bar{x}) \equiv \begin{cases} 1-4\bar{x}^2 & \text{if} -\tfrac{1}{2} < \bar{x} < \tfrac{1}{2} \\ 0 & \text{otherwise.} \end{cases} \tag{7.5}$$

For the second we employed a Gaussian hump having equation

$$F(\bar{x}) = \pm e^{-\alpha\bar{x}^2} \quad \text{for all} \quad |\bar{x}| < \tfrac{1}{2}W, \tag{7.6}$$

where $\alpha = 4\ln 2$. The minus sign in (7.6) permits the use of a dip. Results for NACA 00XX cross-sections will also be reported. For these airfoil sections spline coefficients were determined from the data of Abbott & Doenhoff (1959), from which $F(\bar{x})$ and its derivatives could be computed at any point.

Following Fletcher (1988), we cast (7.1) in conservative form

$$G_{\bar{x}}+H_{\bar{y}} = -\nu\bar{\phi}_{\bar{x}\bar{x}\bar{x}\bar{x}}, \tag{7.7}$$

where the flux functions are defined

$$G \equiv (1-M_\infty^2)\,\bar{\phi}_{\bar{x}}-\bar{\Gamma}\bar{\phi}_{\bar{x}}^2+\frac{\Lambda}{3}\bar{\phi}_x^3, \quad H \equiv \bar{\phi}_{\bar{y}}. \tag{7.8}$$

The finite differencing of the flux functions is a straightforward extension of the method described by Fletcher (1988). The approximated form of the artificial viscosity term is obtained by using two successive applications of central differences on half-grids. The error analysis for the inviscid scheme has been studied extensively by Murman & Cole (1971) and Murman (1973), and we refer the reader to these for further details.

The grid employed has a constant spacing on the wing and then decays geometrically out to the computational boundary in both the $\bar{x}$- and $\bar{y}$-directions. The rate of decay is the same in both directions and ranges from 5 to 15%. The typical number of points distributed over the chord was 40.

The resulting difference equation is found to be a cubic polynomial in $\bar{\phi}_{i,j}$. At each fixed value of $\bar{x}$, or equivalently i, we invert the corresponding nonlinear system of equations using a fully implicit Gauss–Seidel line relaxation technique. We march from left to right in $\bar{x}$ with a complete sweep composing a single iteration. We then compute the L_∞-norm of the residuals and compare with the previous iteration's norm. If this difference is less than a specified tolerance or a maximum number of iterations is reached, the iteration process is terminated, and we use this as the converged solution. The typical tolerance employed was between 10^{-5} and 10^{-6} which required on the order of 4000–5000 iterations with 40 points on the wing.

8. Numerical results

To illustrate the ability of the numerical scheme to approximate the exact solutions to systems (3.17)–(3.19) or (5.3)–(5.5), we have computed the flow over the smooth hump or dip given by (7.6). The value of Λ was taken to be zero so that (3.17) or (7.1) reduced to the classical small-disturbance equation. The main point of these computations was to verify the similitude under changes in the sign of $\bar{\Gamma}$. In the following, we will take $\epsilon = 0.03$ and $M_\infty = 0.867$. The first case considered corresponds to the flow of air ($\bar{\Gamma} = 1.2$) over first a hump and then a dip. The computed pressure distributions have been plotted in figure 9. As expected, the acceleration of the flow over the hump gives rise to a region of supersonic flow which is terminated by a compression shock. When the lower sign in (7.6) is employed, the flow decelerates and the pressure increases in the centre portion ($\bar{x} \approx 0$) of the dip. As one expects, the flow remains subsonic everywhere. We then changed the sign of $\bar{\Gamma}$ and recomputed both solutions with the same grid, number of iterations, and other physical parameters. The results are plotted in figure 10. The flow over the hump now remains entirely subsonic and the flow compression over the dip results in a supersonic flow terminated by the expansion shock seen in figure 10(*b*). By a more detailed inspection of the output, it can be shown that the $\bar{\Gamma} > 0$ flow over the hump (dip) is identical to the $\bar{\Gamma} < 0$ flow over the dip (hump), provided the sign change in c_p is taken into account. This is in complete agreement with the similitude described in §4. Further similitude studies involving $\Lambda \neq 0$ were also carried out and result in the same general conclusion; namely, the numerical scheme at least appears to satisfy the symmetry structure inherent in systems (3.17)–(3.19) and (5.3)–(5.7), even when shocks are present.

The results depicted in figures 9 and 10 are also consistent with Thompson's (1971) remarks concerning the variation of the streamtube areas required to produce supersonic flow. In particular, our results are consistent with Thompson's observation that the streamtubes must form an anti-throat in order to accelerate a $\bar{\Gamma} < 0$ fluid to supersonic conditions.

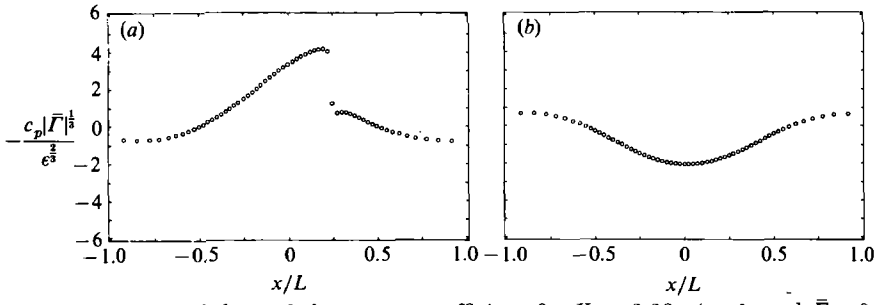

FIGURE 9. Plots of the scaled pressure coefficient for $K_1 \approx 2.28$, $\Lambda = 0$, and $\bar{\Gamma} > 0$. Flow is over the Gausian (*a*) hump, (*b*) dip, given by (7.6).

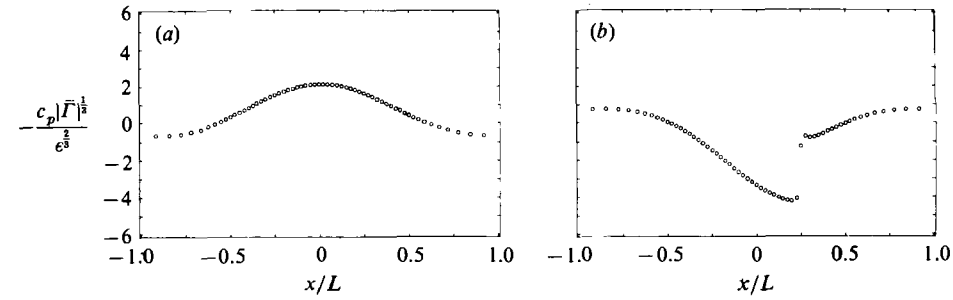

FIGURE 10. As figure 9 but for $\bar{\Gamma} < 0$.

In the next series of calculations, we examined the effect of the second nonlinearity coefficient on the flow details. The circular-arc cross-section (7.5) was employed and ϵ, $\bar{\Gamma}$, M_∞ were fixed at values of 0.02, 0.25 and 0.996, respectively. At $\Lambda = 0$, $K_{1c} \approx 2.86$ and the classical theory predicts a supercritical flow. We then increased the value of Λ from zero to verify the assertion that the critical Mach number increases with increasing Λ, at least in the $\bar{\Gamma} > 0$, $\Lambda > 0$ case. The results are presented in figure 11. Figure 11(*a*) depicts the $\Lambda = 0$ flow which is seen to be strongly supercritical with a large compression shock near the trailing edge. As Λ or K_2 is increased, the compression shock weakens and moves upstream. At $K_2 = 0.52$, the flow is seen to be shock-free. The Mach number distribution corresponding to this value of K_2 is plotted in figure 12 where it is seen that the flow is entirely subsonic. The appearance of the local maximum in M is evident at $\bar{x} \approx -0.125$ and 0.125. This local maximum was found to be approximately 0.995. These results are, of course, consistent with those of §6. For example, inspection of figure 8 reveals that the point $K_1 \approx 2.28$, $K_2 = 0.52$ lies in subsonic region, i.e. $K_1 > K_{1c}$ ($K_2 = 0.52$).

We recall that the quantities $\bar{\Gamma}$ and K_1 are fixed in the series of calculations leading to figure 11. Thus, the increase in M_c is solely due to the non-classical effects. Although $\Gamma > 0$ in the free stream, the fact that $\Lambda > 0$ results in a decrease in the local value of $\bar{\Gamma}$ in the expansive portion of the flow. Ultimately, the local value of Γ becomes negative, which, according to (5.7)–(5.8), results in a decrease in the local Mach number upon further expansion. As long as the local maximum in M is less than one, the flow remains subcritical regardless of the strength of the disturbance.

With the exception of the Mach number variation, subcritical flows of BZT fluids are qualitatively the same as those of perfect gases. However, supercritical flows can

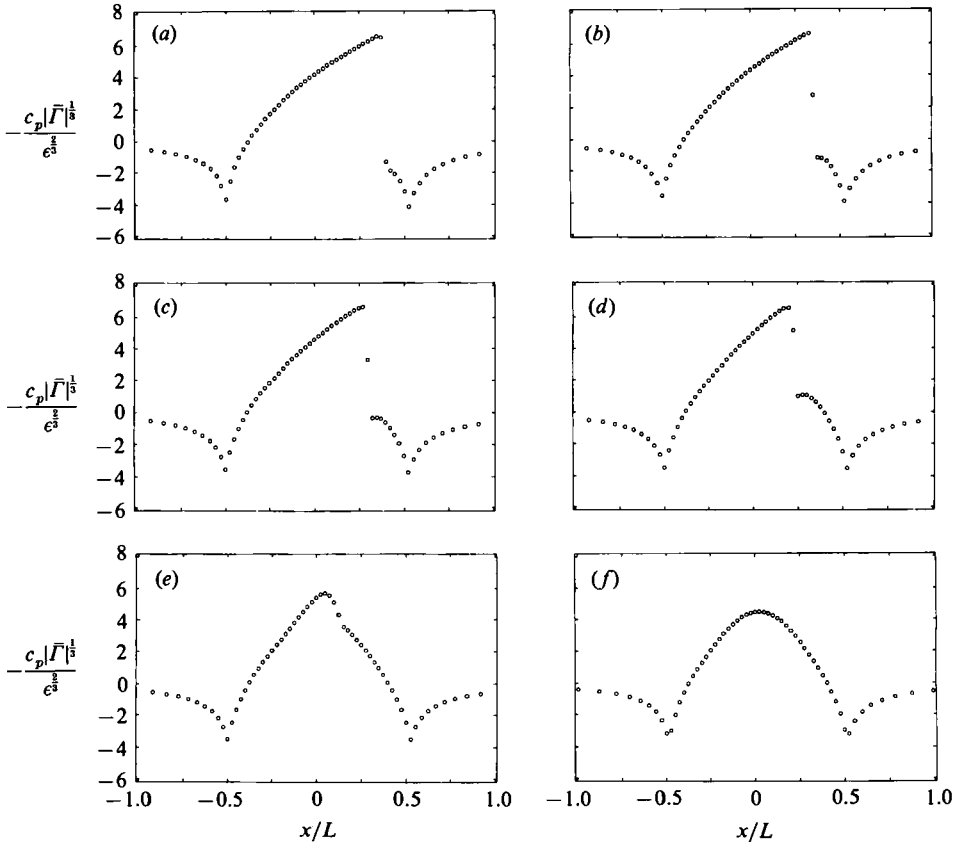

FIGURE 11. Plot of the scaled pressure coefficient for flow over a circular arc airfoil. The similarity parameters are given by $\bar{\Gamma} > 0$, $K_1 \approx 2.28$, and (*a*) $K_2 = 0$, (*b*) $K_2 = 0.104$, (*c*) $K_2 = 0.208$, (*d*) $K_2 = 0.312$, (*e*) $K_2 = 0.416$, (*f*) $K_1 = 0.520$.

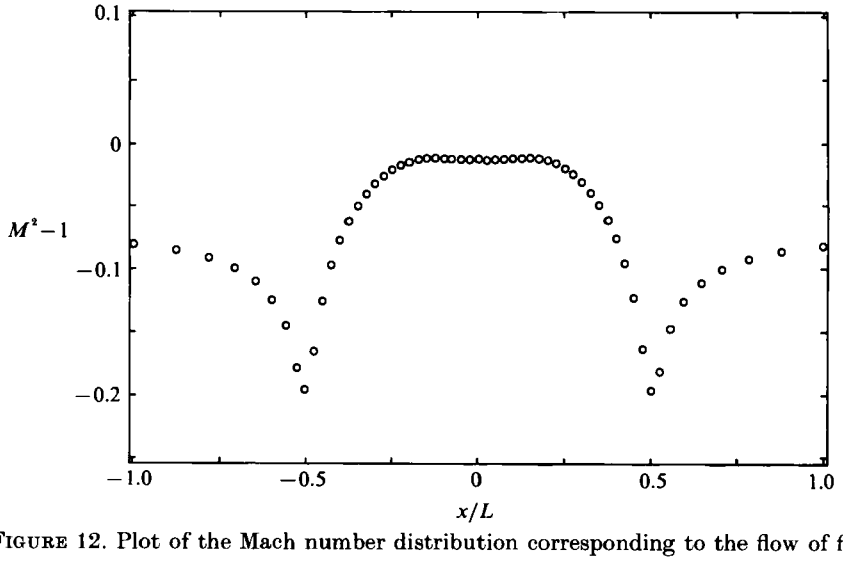

FIGURE 12. Plot of the Mach number distribution corresponding to the flow of figure 11 (*f*).

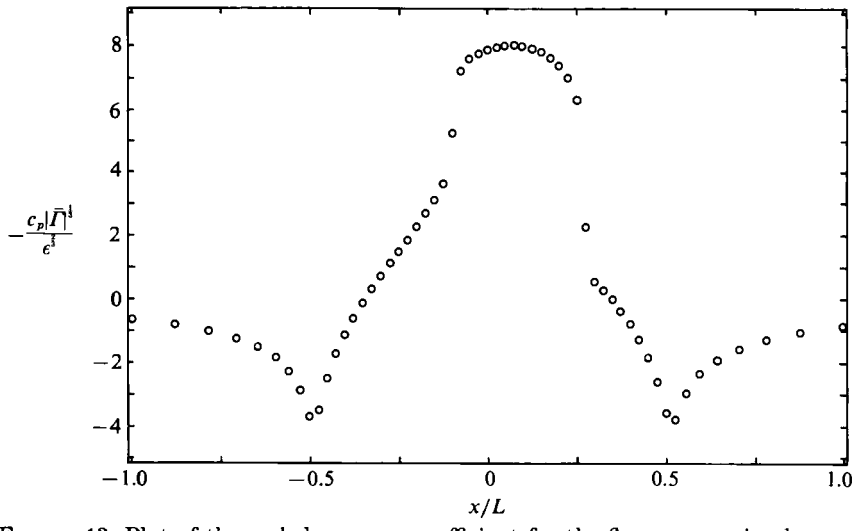

FIGURE 13. Plot of the scaled pressure coefficient for the flow over a circular-arc airfoil. The similarity parameters are given by $\bar{\Gamma} > 0$, $K_1 \approx 1.56$, $K_2 \approx 0.520$.

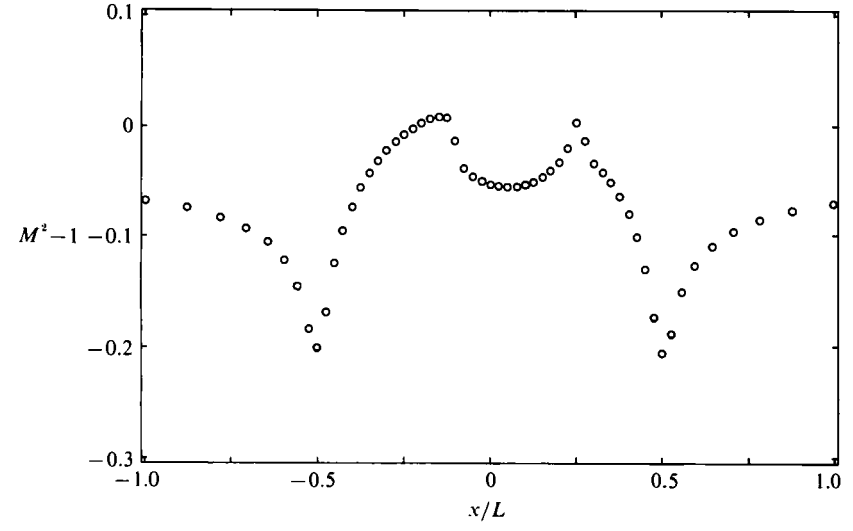

FIGURE 14. Plot of the Mach number distribution corresponding to the flow of figure 13.

be significantly different. As an illustration, we have recomputed the case depicted in figures 11(*f*) and 12 with a Mach number corresponding to supercritical conditions. The pressure and Mach number distributions are plotted in figures 13 and 14. A contour plot of the scaled pressure coefficient is provided in figure 15. We find that two shocks are generated corresponding to the two supersonic regions expected in the vicinity of the local maxima in the Mach number distributions. As the flow expands away from the leading edge, a weak expansion shock is formed. The second shock is of the compression type and is formed downstream of the point of maximum thickness. Both shocks are non-sonic, although sonic shocks can be observed for other parameter choices. The flow pattern containing both expansion and

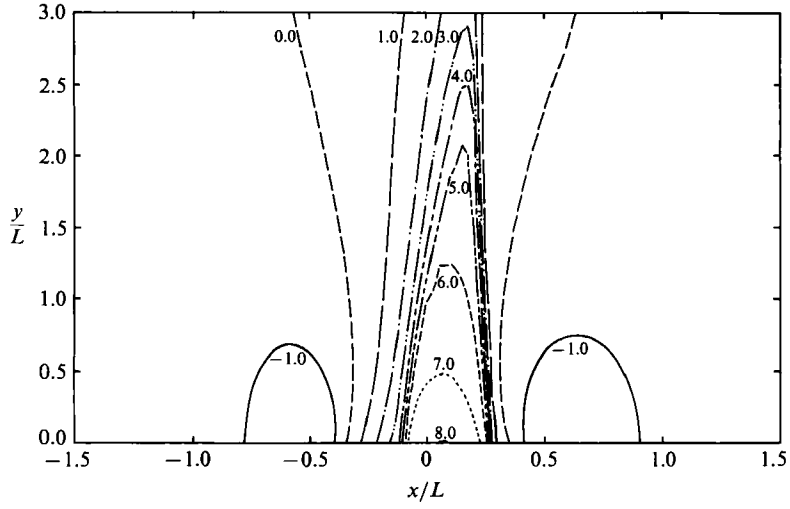

FIGURE 15. Contour plot of $-c_p \bar{\Gamma}^{\frac{1}{3}}/\epsilon^{\frac{2}{3}}$ corresponding to flow of figure 13.

compression shocks is seen to be similar to that predicted by Warner (1990) and Chandrasekar & Prasad (1991) for flows of BZT fluids in converging–diverging nozzles. However, in both of these previous investigations, the compression shock analogous to that seen in figure 13 is necessarily sonic.

Another view of the expansion and compression shock is found in the contour plot of figure 15. The expansion shock is seen to spread and appears to disintegrate entirely before striking the compression shock. With the exception of the steepening near the wing associated with the expansion shock, the flow pattern superficially resembles that of the perfect gas theory, albeit when the latter is applied at lower Mach numbers. However, the values of pressure corresponding to supersonic conditions are given by $2.2 < -\tilde{c}_p < 5.5$. As seen in figure 14, the flow between the expansion and compression shocks is primarily subsonic. It should be clear that a recognition of the non-monotone relation between the Mach number and pressure will be particularly important in the interpretation of contour plots of the Mach number.

Subcritical and supercritical flows over a NACA 00XX cross-section are depicted in figure 16 for $K_1 = 0.342$, 0.684, and 1.368. If we employ the positive value of A given for PP11 in table 1, $\bar{\Gamma} = 0.25$, and $\epsilon = 0.02$, we find that the corresponding Mach numbers are 0.995, 0.990, and 0.980. The plots at $K_1 = 0.342$ and 0.684 were found to be supercritical whereas that at $K_1 = 1.368$ is subcritical. This is in agreement with the theoretical prediction of $K_{1c} = 0.822$. In the supercritical cases, the compression shock is found near the trailing edge. When the Mach number distribution was examined we found that the upstream state for this shock is nearly sonic. We would also expect to see an expansion shock near the leading edge. Such an expansion shock is consistent with the fundamental existence conditions. Furthermore, this expectation is also consistent with an inspection of the corresponding Mach number distributions, and the fact that the expansion remains steep even though the compression shock has already appeared. Unfortunately, the expansion region shown only contains one or two mesh points in spite of the fact that 50 points were (uniformly) distributed over the chord, and no definite conclusion can be made. Inspection of figure 16 also reveals that a large part of the compression on

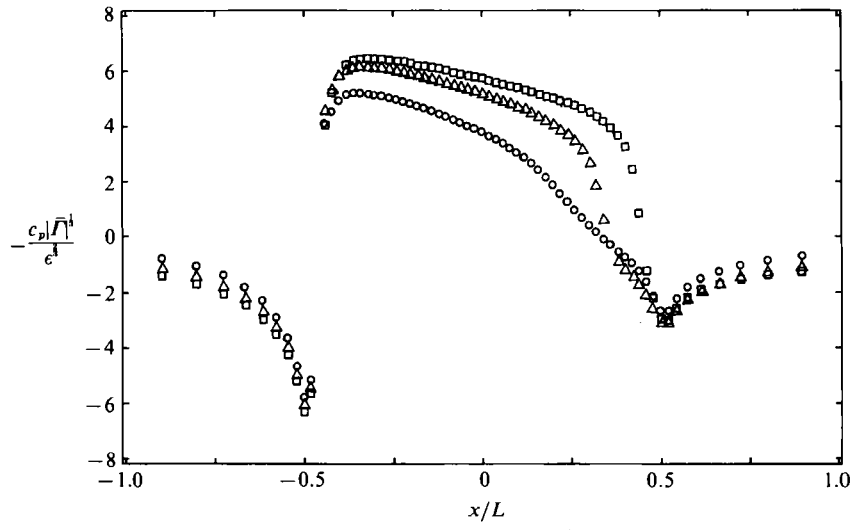

FIGURE 16. Plots of the scaled pressure coefficient for the flow over a NACA 00XX airfoil. The value of $\bar{\Gamma}$ is positive and $K_2 \approx 1.216$. The values of K_1 are: $K_1 \approx 1.368$ (○), $K_1 \approx 0.684$ (△), $K_1 \approx 0.342$ (□).

the NACA 00XX series occurs gradually rather than through a shock. This limitation on the shock strength and associated adverse pressure gradient suggests there may be advantages in the use of BZT fluids even at supercritical speeds.

Analogous computations were carried out by Morren (1991) who presented finite-volume solutions of the Euler equations supplemented with the van der Waals equation of state. When the free-stream state corresponded to that of figures 13–16, structures similar to those found here were obtained. In particular, the grid employed by Morren appears to have better resolution near the nose of the NACA 0012 airfoil and an expansion shock is clearly visible. The gradual compression and reduced strength of the compression shock is also present in Morren's results.

As a final example of the non-classical dynamics of BZT fluids we consider a supercritical flow in which the free stream is still subsonic but which has $\Gamma_\infty < 0$. A circular-arc airfoil with $\epsilon = 0.02$ is employed with $M_\infty \approx 0.995$ and $\bar{\Gamma} = -0.25$, $A = 2.6$. The pressure distribution on the wing is plotted in figure 17 and a contour plot of the pressures is given in figure 18. The novel feature seen here is that a bow shock of the compression type is generated upstream of the leading edge. There also appears to be an expansion shock downstream of the trailing edge. Both the compression and expansion shocks were predicted by Cramer & Best (1991). The physical reason for this bow shock is due to the non-classical variation in the Mach number illustrated in figures 3 and 5(*b*). In the $\Gamma_\infty < 0$ region, the Mach number will initially increase rather than decrease with pressure if $M_\infty \approx 1$. Thus, the large increase in the pressure occurring near the leading edge may drive the flow supersonic. Once the flow is supersonic further compression is likely to result in a shock. A detailed inspection of the Mach numbers generated shows that this is indeed the case. The occurrence of a bow shock is, of course, impossible in the perfect gas theory or, for that matter, in any other in which the Mach number decreases monotonically with increasing pressure. Monotone increases in the pressure then simply decrease the Mach number and regions of supersonic flow ahead of the wing or turbine blade are not generated.

Inspection of the contour plots reveals that the bow shock disintegrates at a finite

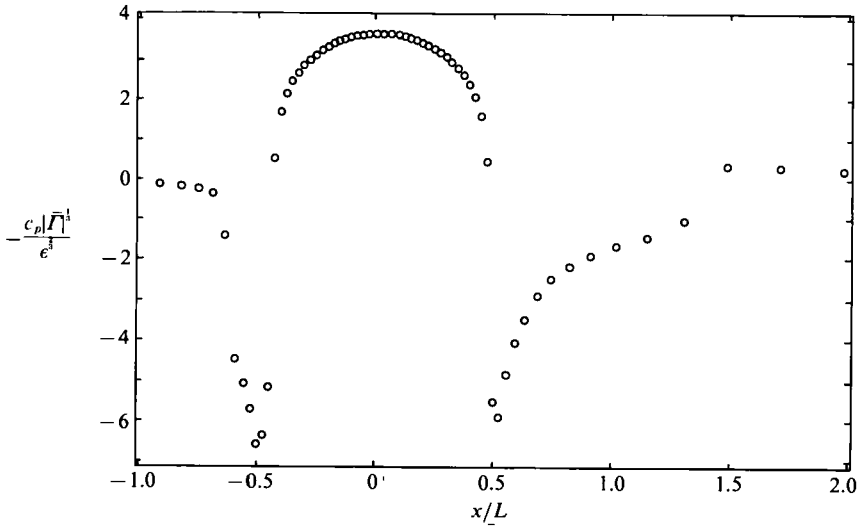

FIGURE 17. Plot of the scaled pressure coefficient over a circular-arc airfoil. The similarity parameters are given by $\bar{\Gamma} < 0$, $K_1 = 0.342$, and $K_2 = 1.216$. The compressive bow shock can be seen between $x = -0.8L$ and $-0.6L$. The wake expansion shock can be seen between $x \approx 1.4L$ and $1.5L$.

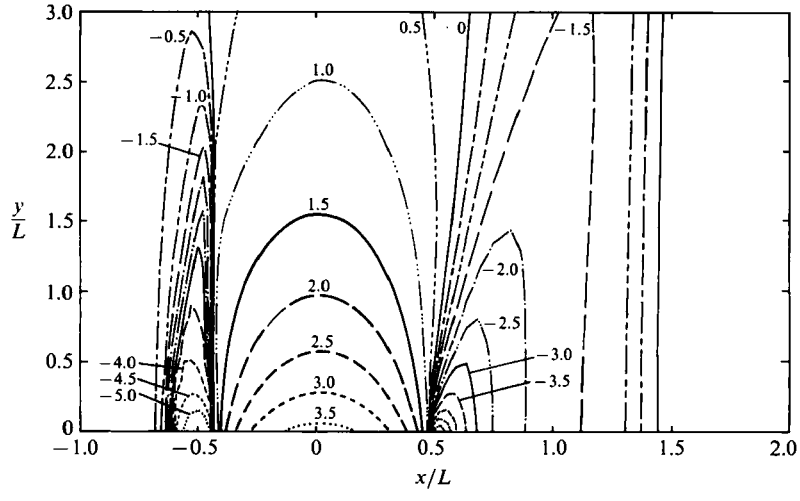

FIGURE 18. Contour plot of $-c_p|\bar{\Gamma}|^{\frac{1}{3}}/\epsilon^{\frac{2}{3}}$ corresponding to the flow of figure 17.

distance normal to the blade. This may be anticipated by noting that the strength of any bow shock decreases with distance from the centreline. In the far-field $\Gamma < 0$ everywhere and the compression shock will violate the basic existence conditions, including the entropy inequality. Thus, such a bow shock will always terminate in the flow. We expect that similar arguments may be applied to show that both attached and detached leading compression shocks should disintegrate if $M_\infty > 1$, $A > 0$, $\bar{\Gamma} < 0$. Arguments for attached oblique shocks in strictly supersonic flows have given by Cramer (1991).

The rapid variations of the flow just downstream of the leading edge and just upstream of the trailing edge are expected to contain expansion and compression

shocks. A detailed inspection of the Mach number distribution shows that each shock is likely to be sonic at the upstream state. Paired sonic expansion and compression shocks were also found by Warner (1990) and Chandrasekar & Prasad (1991) in their studies of nozzle flows.

9. Summary

The work presented here should be regarded as a first step toward understanding the transonic flow of BZT fluids over thin airfoils or turbine blades. The main difference between the present study and the classical small-disturbance theory is that the fundamental derivative is taken to be small. The transonic small-disturbance equation was derived subject to this restriction and was found to include a second nonlinearity parameter related to the variation in Γ with density. The similarity properties of this equation are discussed in §4. It is found that the additional nonlinearity parameters complicate the similitude considerably. Of particular interest is the fact that the value of the usual transonic similarity parameter (1.3) is no longer fixed at the critical conditions. This breakdown in the classical similarity laws is to be expected whenever the fundamental derivative becomes small.

Predictions of the critical Mach number were presented in §6. Very large increases in M_c were reported, particularly when $\Gamma > 0$ and the free-stream thermodynamic state was in the vicinity of the high-pressure zero of Γ. The physical reasons behind these increases are two-fold. The first is due to the decrease in the intrinsic nonlinearity when $\bar{\Gamma}$ is small and could be anticipated through use of the classical similarity parameter (1.3). The second contribution to the increase is entirely non-classical and is because the flow expansion causes the local value of Γ to become negative. As a result, further expansion causes the local Mach number to decrease, thus limiting the maximum value of the local Mach number. This additional increase in M_c due to the non-classical dynamics is particularly evident in calculations of the type summarized in table 2 and in the series of calculations represented in figures 11 and 12.

The results predicted here are expected to give a reasonable approximation to the actual flow provided our original assumptions are valid. We have conducted several numerical tests, both reported and unreported, which have confirmed that a wide range of blade configurations and flow parameters may be found such that the local disturbances remain small and the Mach number variation given here is a good approximation to the actual variation. These cases include those in which large increases in M_c are observed. As discussed in §§5 and 6, the prediction that $M_c = 1$ when $\bar{\Gamma} = 0$ will never be realized in practice owing to the Prandtl–Glauert amplification of the disturbances. Even in these cases, the physical effects leading to the breakdown of the present theory require operation at very large values of M_∞, thus suggesting that the actual limiting value of M_c will still be large although not identically one. Further work is underway by the present authors to improve the estimates of this limiting value.

The flow details were obtained through use of the numerical scheme outlined in §7 and are seen to be in marked contrast to those of the perfect gas theory, particularly in the case of supercritical flows. Qualitatively similar flow patterns were also generated by Morren (1991) who solved the full Euler equations. We again conclude that the general flow features revealed here can be expected to be observed in more accurate numerical calculations or in experimental studies.

This research was supported by the National Science Foundation under grant CTS-8913198. The authors would also like to thank Dr S. A. Ragab for a number of useful suggestions and conversations.

REFERENCES

ABBOTT, R. H. & DOENHOFF, A. E. 1959 *Theory of Wing Sections*. Dover.

ANDERSON, J. D. 1990 *Modern Compressible Flow with Historical Perspective*. McGraw-Hill.

BETHE, H. A. 1942 The theory of shock waves for an arbitrary equation of state. *Office Sci. Res. & Dev. Rep.* 545.

CHANDRASEKAR, D. & PRASAD, P. 1991 Transonic flow of a fluid with positive and negative nonlinearity through a nozzle. *Phys. Fluids* A **3**, 427–438.

COLE, J. D. & COOK, L. P. 1986 *Transonic Aerodynamics*. North Holland.

CRAMER, M. S. 1987 Structure of weak shocks in fluids having embedded regions of negative nonlinearity. *Phys. Fluids* **30**, 3034–3044.

CRAMER, M. S. 1989*a* Negative nonlinearity in selected fluorocarbons. *Phys. Fluids* A **1**, 1894–1897.

CRAMER, M. S. 1989*b* Shock splitting in single-phase gases. *J. Fluid Mech.* **199**, 281–296.

CRAMER, M. S. 1991 Nonclassical dynamics of classical gases. In *Nonlinear Waves in Real Fluids* (ed. A. Kluwick), pp. 91–145. Springer.

CRAMER, M. S. & BEST, L. M. 1991 Steady isentropic flows of dense gases. *Phys. Fluids* A **3**, 219–226.

CRAMER, M. S. & CRICKENBERGER, A. B. 1991 The dissipative structure of shock waves in dense gases. *J. Fluid Mech.* **223**, 325–355.

CRAMER, M. S. & KLUWICK, A. 1984 On the propagation of waves exhibiting both positive and negative nonlinearity. *J. Fluid Mech.* **142**, 9–37.

CRAMER, M. S., KLUWICK, A., WATSON, L. T. & PELZ, W. 1986 Dissipative waves in fluids having both positive and negative nonlinearity. *J. Fluid Mech.* **169**, 323–336.

CRAMER, M. S. & SEN, R. 1987 Exact solutions for sonic shocks in van der Waals gases. *Phys. Fluids* **30**, 377–385.

DUHEM, P. 1909 Sur la propagation der ondes de choc au sein des fluides. *Z. Phys. Chem, Leipzig* **69**, 169–186.

FLETCHER, C. A. G. 1988 *Computational Techniques for Fluid Dynamics*. Springer.

HAYES, W. D. 1966 La seconde approximation pour les écoulements transsoniques non visqueux. *J. Méc.* **5**, 163–206.

KEVORKIAN, J. & COLE, J. D. 1981 *Perturbation Methods in Applied Mathematics*. Springer.

KLUWICK, A. & KOLLER, F. 1988 Ausbrietung periodischer Wellen kleiner Amplitude in Gasen mit großen specifischen Wärmen. *Z. Angew. Math. Mech.* **68**, T306–T307.

LAMBRAKIS, K. & THOMPSON, P. A. 1972 Existence of real fluids with a negative fundamental derivative Γ. *Phys. Fluids* **5**, 933–935.

LANDAU, L. D. & LIFSHITZ, E. M. 1959 *Fluid Mechanics*. Addison-Wesley.

LEIDNER, P. 1990 Realgaseinflüsse in der Gasdynamik. Diplomarbeit, Universtät Karlsruhe.

MARTIN, J. J. & HOU, Y. C. 1955 Development of an equation of state for gases. *AIChE J.* **1**, 142–151.

MENIKOFF, R. & PLOHR, B. 1989 Riemann problem for fluid flow of real materials. *Rev. Mod. Phys.* **61**, 75–130.

MORREN, S. H. 1991 Transonic aerodynamics of dense gases. *NASA TM* 103732.

MURMAN, E. M. 1973 Analysis of embedded shock waves calculated by relaxation methods. *Proc. 1st AIAA Comp. Fluid. Dyn. Conf.*, pp. 27–40.

MURMAN, E. M. & COLE, J. D. 1971 Calculation of plane steady transonic flow. *AIAA J.* **9**, 114–121.

NIEUWLAND, G. Y. & SPEE, B. M. 1973 Transonic airfoils: Recent development in theory, experiment, and design. *Ann. Rev. Fluid Mech.* **5**, 119–150.

PEGO, R. L. 1986 Nonexistence of a shock layer in gas dynamics with a nonconvex equation of state. *Arch. Rat. Mech. Anal.* **94**, 165–178.

REID, R. C., PRAUSNITZ, J. M. & POLING, B. E. 1987 *The Properties of Gases and Liquids*, 4th Ed, Wiley.

SOBIECZKY, H. & SEEBASS, A. R. 1984 Supercritical airfoil and wing design. *Ann. Rev. Fluid Mech.* **16**, 337–363.

THOMPSON, P. A. 1971 A fundamental derivative in gasdynamics. *Phys. Fluids* **14**, 1843–1849.

THOMPSON, P. A. & LAMBRAKIS, K. 1973 Negative shock waves. *J. Fluid Mech.* **60**, 187–208.

WARNER, S. M. 1990 Steady non-isentropic flows of dense gases, *Virginia Polytechnic Institute and State University Engineering Rep.* VPI-E-90-24.

WENDROFF, B. 1972 The Riemann problem for materials with nonconvex equations of state II: General flow. *J. Math. Anal. Applics* **38**, 640–658.

ZEL'DOVICH, YA. B. 1946 On the possibility of rarefaction shock waves. *Zh. Eksp. Teor. Fiz.* **4**, 363–364.